INVESTIGATION OF MECHANICAL AND TRIBOLOGICAL BEHAVIOUR OF GRAPHENE NANOPLATELET REINFORCED ZE10 MAGNESIUM ALLOY

A Thesis Submitted to
the Graduate School of
İzmir Institute of Technology
in Partial Fulfillment of the Requirements for the Degree of

MASTER OF SCIENCE

in Mechanical Engineering

by

Sibel YÖYLER

March 2022
IZMIR

ACKNOWLEDGMENTS

First of all, I would like to thank my advisor Assoc. Prof. Sinan Kandemir for the useful comments and his guidance through the learning and writing process of my master thesis. I would like to thank my co-advisor Dr. Maksim Antonov who is the head of Research Laboratory of Tribology and Materials Testing at Tallinn University of Technology (TalTech) for giving me the opportunity to work in their laboratory, sharing his knowledge and his kindness. I am also grateful to the other members of my thesis defense committee, Assoc. Prof. Fatih Toptan, Assoc. Prof. Onur Ertuğrul for their suggestions. I would like to thank Helmholtz Zentrum Hereon which is located in Geesthacht, Germany to provide casting samples which are used in this research.

My deepest gratitude goes foremost to my father Ender Yöyler who has given his unconditional love and endless encouragement to me. He has always been understanding and supportive all over my education life. Also, I warmly thank my mother Güzel Aysel who is supporting the decisions I made, encouraging and moralizing me. I would like to thank my brothers Sidan Yöyler, and Murat Yöyler for being there for me all the time and believing me. I am happy to dedicate the thesis to my family. This accomplishment would not have been possible without them.

I would also like to thank Rahul Kumar who was a Ph.D. student at TalTech for his help and knowledge. I would like to express my gratitude to Mansure Rezapourian who is a Ph.D. student at TalTech for her continuous support guidance and valuable friendship. We have spent enjoyable tea breaks together which made me feel more and more confident and cheerful.

I would like thank to my friend Işılay Öztürk who has always encouraged me to do my best. I could not have imagined having a better mentor. I also would like to thank my friends Kelsüme Savcı and Arife Bağış for their precious friendship. They have always motivated me to conduct my research and write my thesis. I would like thank to Hacer İrem Erten for all the memories and support which have motivated me throughout this thesis. Lastly, a heartfelt thank you to the many people who went unmentioned but made a significant contribution to the success of the study in some way.

ABSTRACT

INVESTIGATION OF MECHANICAL AND TRIBOLOGICAL BEHAVIOUR OF GRAPHENE NANOPLATELET REINFORCED ZE10 MAGNESIUM ALLOY

Since graphene was discovered, it has increased the hopes of improving and widening the usage areas of metal matrix composites with its unique mechanical properties. Graphene nanoplatelets (GNPs) was reinforced into the matrix in this study. The added GNPs have approximately 10-20 nm thickness and 14μm diameter. 0, 0.25, 0.5, and 1.0wt.%GNPs were incorporated in the matrix, which is ZE10 Mg alloy. Compared to pure magnesium, ZE10 alloy has better ductility, formability, creep resistance, and corrosion resistance thanks to the rare earth elements. The stir casting method is demanded in industry owing to its suitability for making products complex-shaped in large sizes. The combination of stir casting and ultrasonic processing was employed. Due to the high surface energy of nanosized GNP reinforcement, high energy mixing is required effectively to ensure homogeneous distributions. Therefore, ultrasonic processing was applied along with stir casting. This study aims to investigate the microstructure, mechanical properties, and wear behavior at various temperatures of ZE10 alloy with reinforced GNP. The microstructure examination, ball-on-disc, hardness, and tensile tests were performed on the cast reference alloy without GNP and composites. Ball-on-disc and hardness tests were performed at room temperature, 100 °C and 200 °C. It was observed that obtaining a homogeneous distribution became more difficult with the increased GNP content in the optical microscope images. The composite with 0.25 wt. %GNP content has the smallest grain structure compared to composites with different content of GNP (0.5 and 1.0 wt.%GNP). It was also observed that adding 0.25 wt. % GNP improved the wear and hardness values 8,1% and 22% at room temperature, respectively. Adhesive and abrasive mechanisms were proposed to be the principal wear mechanisms in consequence of the existence of delicate furrows, and plowing marks.

ÖZET

GRAFEN NANOLEVHA TAKVİYELİ ZE10 MAGNEZYUM ALAŞIMININ MEKANİK VE TRİBOLOJİK DAVRANIŞLARININ İNCELENMESİ

Grafen, benzersiz mekanik özellikleri ile metal matrisli kompozitlerin kullanım alanlarını ve gelişme umutlarını arttırmıştır. Grafen nanolevhalar (GNL) bu çalışmada matrise takviye edilmiştir. Eklenen GNL'lar yaklaşık 10-20 nm kalınlığa ve 14 μm çapa sahiptir. ZE10 Mg alaşımına ağırlıkça yüzde 0, 0.25, 0.5 ve 1.0 GNL'lar dahil edilmiştir. Saf magnezyum ile karşılaştırıldığında, ZE10 alaşımı içerdiği nadir toprak elementleri sayesinde daha iyi süneklik, şekillendirilebilirlik, sürünme direnci ve korozyon direncine sahiptir. Karıştırmalı döküm yöntemi, büyük boyutlarda karmaşık şekilli ürünler yapmaya uygunluğu nedeniyle endüstride talep edilmektedir. Nano boyutlu GNL takviye elemanının yüksek yüzey enerjisi nedeniyle, homojen dağılımını sağlamak için yüksek enerjili karıştırma gereklidir. Bu yüzden ultrasonik işlem ile karıştırmalı döküm birlikte uygulanmıştır. Bu çalışma, GNL takviye edilmiş ZE10 Mg alaşımının mikro yapısını, mekanik özelliklerini, farklı sıcaklıklardaki sertlik ve aşınma davranışlarını incelemeyi amaçlamaktadır. GNL içermeyen referans alaşım ve kompozitler üzerinde mikroyapı incelemesi, disk üzeri bilye tipi aşınma, sertlik ve çekme testleri gerçekleştirilmiştir. Disk üzerinde bilye tipi aşınma ve sertlik testleri, oda sıcaklığı, 100 °C ve 200 °C de gerçekleştirildi. Optik mikroskop resimlerinde GNL oranının artması ile homojen dağılımı elde etmenin zorlaştığı görüldü. Ağırlıkça %0.25 GNL oranına sahip kompozit, farklı GNL (0.5 ve 1.0% GNL) oranlarına sahip kompozitlere göre en küçük tane yapısına sahiptir. ZE10/0.25% GNL kompozitinde, aşınma ve sertlik değerlerinde oda sıcaklığında sırasıyla %8,1 ve %22 iyileşme gözlemlenmiştir. İnce çizgiler ve sürme izleri nedeniyle, ana aşınma mekanizmalarının abrasif ve adhesif aşınma mekanizmaları olduğu öne sürülmektedir.

TABLE OF CONTENTS

LIST OF FIGURES

Figure **Page**

LIST OF TABLES

CHAPTER 1

INTRODUCTION

Lightweight and strong materials are in high demand for structural and mechanical applications in the environment of today. It is known that using lightweight materials contributes to reducing vehicle weight, and thus reducing CO_2 emissions. CO_2 emissions accumulate in nature and cause the air to warm up due to factors such as increasing industry, electricity generation systems, and the number of cars used in transportation. The growth in the number of automobiles on the road is known to be one of the major factors contributing to the increase in CO_2 levels in the atmosphere [1]. Since reducing vehicle weight has been widely accepted to be the most reasonable approach to cut emissions in the automobile industry, lightweight materials such as composites are becoming increasingly popular as alternatives to the conventional denser materials such as steel.

The failure in considering tribological fundamentals in design and manufacture results in significant economic losses, such as shortened equipment life, and substantial energy costs [2]. Machine elements are scrapped for a variety of reasons, the most common of which is wear. Lubrications, are one of the solutions, of contact bodies that are employed in machine elements to minimize wear and energy losses [2]. In some cases, friction may need to be increased rather than reduced. For example, high friction coefficients in brake and clutch materials are desired [3].

Economic cost reduction is possibly achieved by making a good material selection, and increasing material wear resistance by two times [4]. In terms of manufacturing efficiency, cost reduction also plays a significant role. The demand for lightweight and low-wear materials has cleared the path for research into new materials, such as composites, that can be employed in the industry [5].

Composites have been the subject of numerous investigations. Metal matrix composites (MMCs) are projected to play an important role in the future based on the findings of the investigations. Simultaneously, when industrial demands are addressed, demand is on the rise, particularly in the usage of metal-based materials [4]. MMCs can improve properties of metals with the addition of appropriate reinforcement material, thus

increasing their usage areas [6, 7]. As a result, MMCs are expected to produce materials with desired mechanical performance.

When considering metal-based materials, Mg and its alloys are becoming more popular as they are the lightest structural metals [4, 8]. Magnesium alloys have high specific strength, good castability with relatively low melting temperature (approximately 650 °C), and high damping capacity [8]. However, Mg and its alloys generally have limited strength and ductility [8]. One of the preferred methods to increase the wear performance and strength of Mg alloys is to strengthen them with a suitable reinforcement material and fabrication technique, namely composite technology.

Because of its exceptional mechanical properties, graphene has emerged as one of the most promising carbon-based reinforcing materials since its creation in 2004 [9]. Graphene nanoplatelets (GNPs), which are made up of a few layers of graphene, were employed as the reinforcement material in this study. Furthermore, the layered structure of GNPs might be easily sheared owing to the weak van der Waals bonds, therefore it is possible that incorporating GNPs into metals will provide a solid lubricating influence on contact surfaces and increase wear resistance [10].

This study examines the mechanical and tribological behavior of graphene nanoplatelet reinforced ZE10 magnesium alloy with tensile tests at room temperature, ball-on-disc, and hardness tests at various temperatures.

CHAPTER 2

LITERATURE REVIEW

2.1. Composites

Composite materials can be described as artificial materials created by combining two or more materials. They are basically made to improve at least one properties of the traditional materials [7]. These properties can be specific strength, thermal and electrical conductivity, wear and corrosion resistance [7].

Composites consist of two basic phases which are matrix and reinforcement. The main function of reinforcement material is to carry load and increase stiffness and strength of matrix [7]. The functions of matrix in composite include protecting reinforcements, which are usually brittle, against external and environmental effects, transmitting load to reinforcing elements, and holding the entire composite structure together [7]. The properties of a composite are determined by the following key factors; properties of the reinforcement and matrix material, adhesion ability at the reinforcement-matrix interface, reinforcement/matrix ratio, the geometry of the reinforcement [7, 11].

Composite materials are used in a broad range of fields due to their structure and qualities. The product flexibility of composite materials is a significant benefit because each industry has its own set of requirements and expectations [12]. The strength/density ratios of composites are generally higher than traditional materials. For instance, composite profiles with good mechanical qualities can be manufactured and applied to constructions [12]. Composites can be used to create complex machine elements with multiple pieces in one piece such as engine blocks, cylinder heads, or intake manifolds [5, 13]. As a result of the reduced number of parts, the production time is lowered due to the elimination of interconnecting details and pieces [13].

Composites can be classified according to matrix and reinforcement types. A simple diagram showing the classification of composites based on matrix material is shown in Figure 2.1. Matrix materials can be used as metal, ceramic, or polymer

materials, depending on the purpose of application [7]. Therefore, in this classification type, composites are called depending on using the type of matrix.

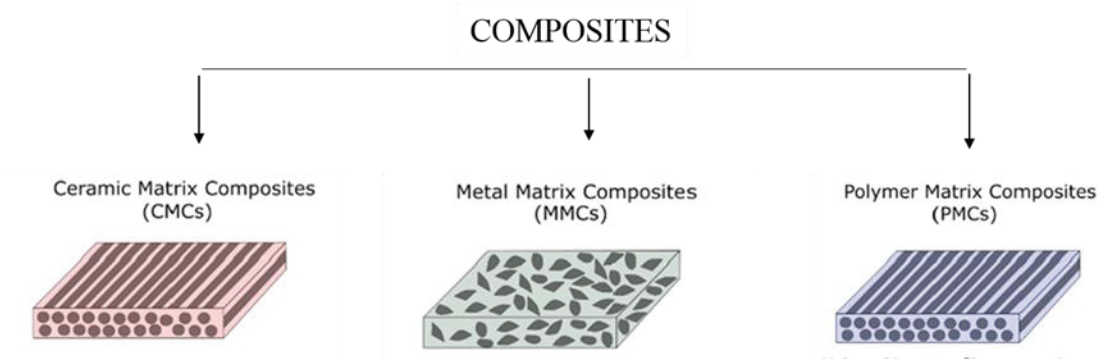

Figure 2.1. Classification of composites based on matrix material [14].

The focus of this research is on MMCs. As a result, the following section heading describes and provides information regarding MMCs, their properties, and manufacturing processes.

2.1.1. Metal Matrix Composites (MMCs)

Composites whose main materials are various metals and metal alloys are called metal matrix composites. Several metals such as Aluminum (Al), Magnesium (Mg), Copper (Cu), Iron (Fe), Titanium (Ti) and their alloys can be employed as the matrix. The reinforcing elements can be ceramic and metallic.

MMCs can operate at higher temperatures compared to their unreinforced matrices. The reasons for choosing MMCs instead of monolithic alloys can be listed as follows [12]:

1. Weight reduction to the high strength to density ratio (specific strength),
2. Higher wear, and fatigue resistance,
3. Dimensional stability,
4. Elevated temperature stability, i.e., creep resistance.

Materials with high abrasion resistance and tensile strength can be created by combining the high modulus of elasticity of ceramics and the plastic deformation capabilities of metals [7].

Reinforcements can be of various geometric shapes and sizes [15]. Particles, continuous and discontinuous fibers, and whiskers can all be used as reinforcements. According to reinforcement geometry, MMCs can be grouped as follows (Figure 2.2); [15]

- Particle reinforced MMCs
- Short fiber reinforced MMCs
- Continuous fiber or sheet reinforced MMCs

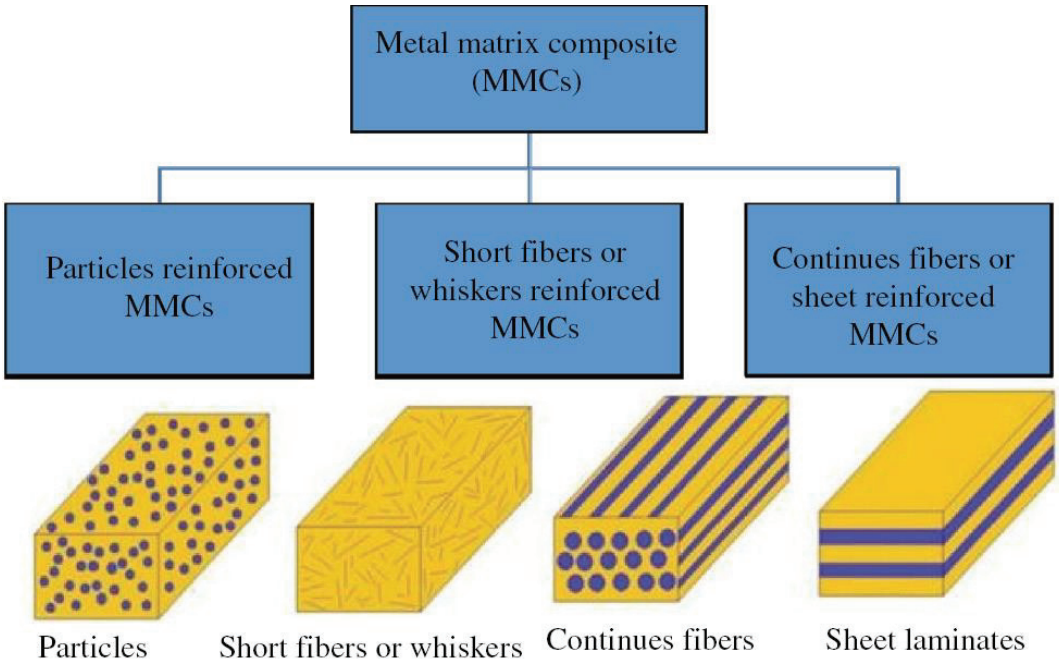

Figure 2.2. Classification of metal matrix according to reinforcement type [15].

Since, particle-reinforced composite materials are topic of this study used, they will be examined in detail under the next heading.

2.1.2. Particulate Reinforced Metal Matrix Composites (PMMCs)

Particles, which can be incorporated into a matrix, can be micron-sized or nano-sized. Particle reinforcing elements can be spherical, cubic, uniform or particles with different types of geometries randomly distributed or oriented in the matrix [6]. Mostly, ceramic particles embedded in a metal matrix have a higher toughness and temperature

resistance [6, 13]. Alongside size and volume percentage of reinforcing elements, the interaction between matrix and reinforcement is known to influence resulting properties of MMCs [11]. Once thin and thermally stable ceramic particles are uniformly distributed in the metal matrix, mechanical properties can be maximized [16]. The cost-effectiveness, isotropic characteristics, and ability to be produced using monolithic technology make particle-reinforced MMCs appealing [6].

2.1.2.1. Reinforcement Type

Reinforcement is more rigid and durable than the matrix in general [7]. The main purpose of the reinforcement is to support the matrix structure, to carry of the incoming load and to increase the material volume [17]. Form, type, ratio, distribution and direction of the reinforcement in the structure, which can be found in continuous or random arrangements in the matrix, significantly affect the composite strength [7]. A major portion of the load on the composite is conveyed by the reinforcing element. The particle reinforcing elements popular used in MMCs are aluminum oxide (Al_2O_3), titanium diboride (TiB_2), silicon carbide (SiC), titanium carbide (TiC), tungsten carbide (WC), boron carbide (B_4C), wolfram (W), and carbon-based (graphene, carbon nanotube, et cetera) materials [16, 18].

Low density, high modulus and strength, ease of production, chemical compatibility with the matrix, and high-temperature resistance are the basic features required from the reinforcement in an MMC, depending on the application [3].

While producing MMC materials, the selection of the reinforcement, the production technique, the ability of the reinforcement to be wetted by the matrix during production, the structural features of the reinforcements determine the physical and mechanical properties of the composite material [8, 13]. For this reason, the correct selection of the reinforcement and its properties should be well known.

MMCs can use continuous fibers, whiskers, short fibers, and particles as reinforcement materials. The aspect ratio is the metric that distinguishes these various sorts of reinforcements [13]. The aspect ratio is the proportion of a fiber's length to its diameter or thickness [13]. The aspect ratio of continuous fibers approaches infinity, but the aspect ratio of totally equiaxed particles is approximately one [13]. Table 2.1 lists some of

the most common reinforcements of MMC, and also their length/diameter (aspect ratios) and diameters. Ceramic reinforcing elements have high elastic modulus and strength, as well as the capacity to withstand high temperatures. Ceramic continuous fibers are more expensive than ceramic particle reinforcements [13].

Table 2.1. Type of reinforcements used in MMCs [13].

Type	**Aspect Ratio**	**Diameter, µm**	**Examples**
Particle	1-4	1-25	SiC, Al_2O_3, BN, B_4C, WC
Short fiber or whisker	10-10000	1-5	C, SiC, Al_2O_3, Al_2O_3+SiO_2
Continuous fiber	>1000	3-150	SiC, Al_2O_3, C, B, W, Nb-Ti, Nb_3Sn

In addition to ceramic reinforcement materials, carbon-based reinforcement materials such as graphite, graphene, are a promising option for raising the mechanical properties of the matrix material, thanks to their high thermal conductivity, high damping capacities and low thermal expansion coefficients [19, 20]. Furthermore, due to their solid lubricant effect, carbon-based reinforcement materials are also widely used to reduce COF and improve the wear behavior of matrix material [10]. However, there are certain limitations in the use of graphite as a reinforcement material. Firstly, graphite needs a humid environment to show the solid lubricant feature [10]. The reason for providing a low coefficient of friction in humid environments is the penetration of water molecules between the graphite sheets so that the graphite sheets are easily sheared and the friction coefficient is reduced by covering the worn surface [10, 21]. On the other hand, it has no major effect on reducing the friction coefficient and wear rate in a dry or vacuum environment [10]. Additionally, numerous researches [22, 23] revealed that the mechanical properties of the matrix material are adversely affected depending on the graphite content. The critical point to consider while selecting the reinforcement material is that mechanical properties are not compromised while improving wear behavior [10, 22]. Several studies showed that the addition of nano-sized reinforcement which is ceramic and/or carbon-based materials to metal matrices can be increased their wear resistance and strength [8]. Lian-Yi Chen et al. [24] produced 6 vol.% SiC in Mg-Zn matrix by casting method by combining semi-solid-state mixing and ultrasonic mixing, and investigated the homogeneous distribution of the nano reinforcement and its effect on the mechanical

behavior of the composite. In the results, they observed that the addition of nanoparticles increased the hardness [24]. Aqeel Abbas et al. [25] added multiwalled carbon nanotubes to the AZ31 Mg alloy using the stir casting method. They suggested that the added nano reinforcements increased the hardness value, and this was due to the homogeneous distribution [25]. Liqun Wu et al. [26] added nickel-coated GNPs as a reinforcing element into the AZ31 matrix and used the vacuum hot pressing method during the production of composites. They indicated that the added nickel-coated GNPs provided improvements in microstructure, mechanical properties, and wear performance compared to the reference AZ31 alloy [26].

Graphene

Graphene is known as a material, which is formed by the arrangement of carbon atoms connected by the covalent bond in a hexagonal lattice with a two-dimensional structure [27]. Graphene can be found as a single layer, several layers, or as a graphitic structure [21]. Graphite, fullerene and carbon nanotubes can also be obtained as a result of variations such as rolling or overlapping of graphene. Figure 2.3 shows a schematic drawing of graphene, fullerene, carbon nanotube, and graphite.

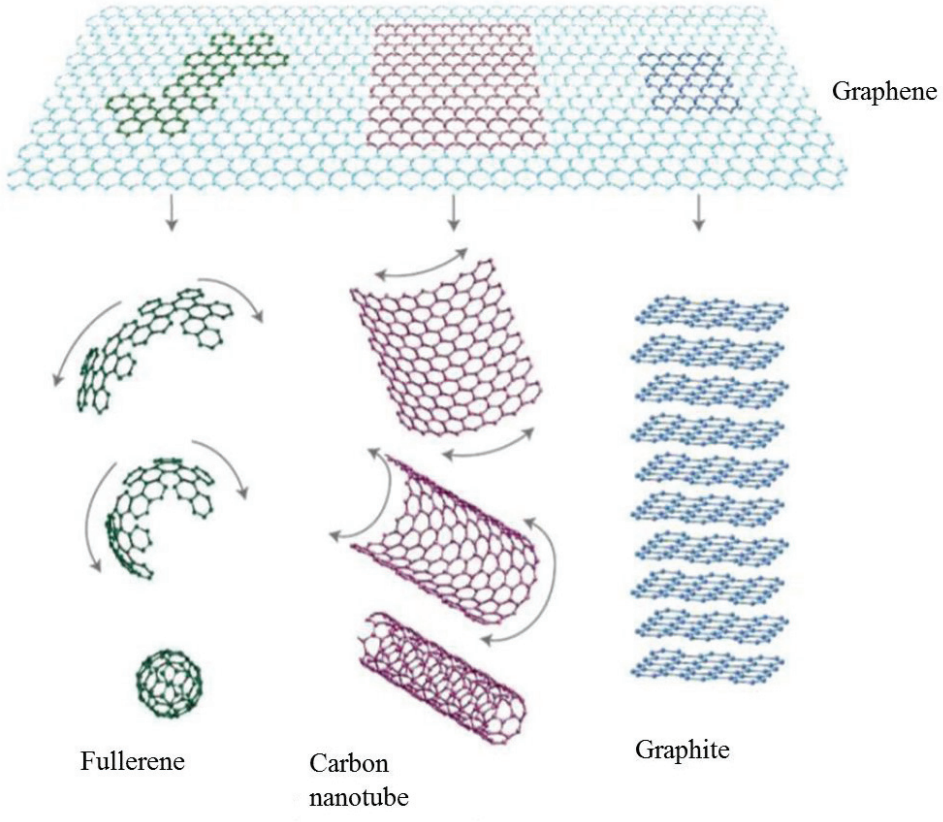

Figure 2.3.Schematic drawings of graphene, fullerene, carbon nanotube, and graphite [18].

Following its synthesis in 2004, graphene has been approved as a reinforcing material with promising and desirable capabilities for various matrices, including polymers, due to its superior electrical, thermal, mechanical, and light weight properties [20, 28].

Graphene has a relatively stable structure with a C–C bond length of only 0.142 nm [27]. Graphene has an extremely strong bond between its carbon atoms [10]. When graphene is exposed to an external force, the atomic surface within it deforms and bends to counteract the force [29]. As a consequence that the carbon atoms do not misalign or rearrange, resulting in a continuously stable structure [29]. There is no scattering of graphene electrons as they travel in the internal orbit due to interference from external atoms or lattice imperfections. Graphene has a variety of remarkable features due to its unique lattice structure [29]. Table 2.2 is shown some properties of graphene.

Table 2.2. Some properties of graphene.

Properties	**Graphene**
Thermal conductivity	4840-5300 $Wm^{-1}K^{-1}$
Elastic modulus	1~ TPa
Fracture strength	130 GPa
Specific surface area	2600 m^2 g^{-1}

GNPs, which are more stable and easier to manufacture compared to graphene, are composed of a few graphene layers [30, 31]. The layered structure of GNPs with weak van der Waals bonds can be easily cut [20, 31, 32]. Therefore, the GNPs into metals can be expected to exert a solid lubricating impact on the surfaces of contact to decrease on wear and friction [32]. In addition, layers of graphene can act as a barrier to crack propagation, thereby decreasing volume loss and counteracting cracking during shearing [30]. The homogeneous distribution of graphene in the composite may provide the desired strength and properties to the composite [33].

2.1.3. The Strengthening Mechanisms

Strengthening mechanisms can explain the enhancement in the mechanical properties of composite materials because of preventing movement of dislocations in the microstructure [34]. Since MMCs have nanoparticle reinforcement in this study, this section will focus on the strengthening mechanism of nano-reinforced MMCs. Four individual strengthening mechanisms were suggested for increasing the mechanical properties of nano-sized reinforced MMCs. These are Hall-Petch (grain size reduction strengthening), Orowan strengthening, the mismatch of the coefficient of thermal expansion (CTE), and the load-bearing effect. These four strengthening mechanisms are explained below.

Since grain boundaries can obstruct movement of dislocation, grain size has a significant impact on metal strengthening [34]. Dislocations cannot find a continuous slip plane for moving in these areas in consequence of the termination of the crystalline structure and the occurrence of a nonuniform structure at the grain boundaries [34]. Another

reason that the grain size affects the movement of dislocations is the orientation differences between the grains [13]. The fact that the grain on the other side of the boundary is positioned at a different angle, obstructs the dislocations from crossing to the other side of the boundary and continuing its movement [13]. When the amount of grain boundary increases, dislocations come across more obstacles so the amount of motionless dislocation increases [13]. This situation causes the strengthening of the material. The way to increase the amount of grain boundaries is to reduce the grains size in the material. Simply, the material has strengthened since grain boundaries are increasing with decreasing the grains size. On the other hand, dislocations sliding in the same slip plane aggregate close by the grain boundary during deformation, forming the dislocation pile-up [34]. Dislocations can apply force to the dislocations in front of the pile-up when new dislocations come to the resulting dislocation pile-up [34]. This situation can allow first-come dislocations to cross over to another grain and continue to slide and this can have a favorable impact on the deformation ability of the material [13]. Dislocation pile-ups in front of the grain boundary remain small when the grain size is reduced. Therefore, a sufficient effect cannot be created to push the dislocations, which are in front of the grain boundary, to the other grain. While this causes the material to become further strengthening, it can adversely affect the deformation capacity of the material [13].

When the relationship between the grain size of the material and the yield strength is examined, it can be said that as the grain size decreases, the yield strength of the material increases [13]. The effect of yield stress and grain size can be shown using the Hall-Petch equation.

$$\sigma_y = \sigma_0 + \frac{k}{\sqrt{d}} \tag{2.1}$$

In this expression, termed the Hall–Petch equation, σ_y is yield stress, σ_0 is the necessary stress for starting dislocation motion, k is a constant, and d is the average grain diameter.

Some obstacles in the crystal tend to avoid dislocation motions (slippage). One of these obstacles is the second phase particles. Dislocations try to keep their mobility by cutting these obstacles if they are weak [34]. However, if there are strong obstacles, they will continue to move by looping around the particle [34]. Orowan strengthening mechanisms are dislocation loops that occur around particles [34]. Figure 2.4 is shown the schematic Orowan strengthening mechanism.

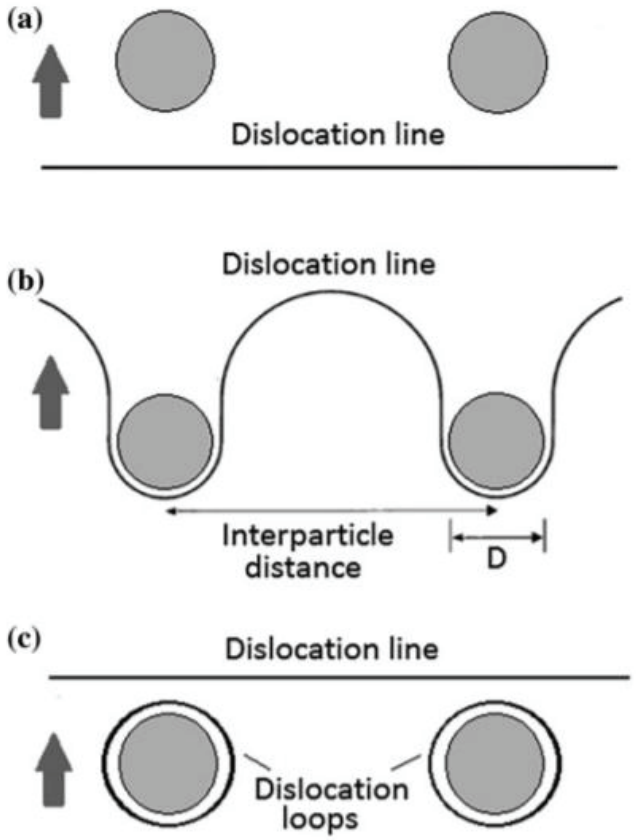

Figure 2.4. Schematic of Orowan strengthening mechanism [34] a) Dislocation line move on towards particles, b) Dislocation line is trying to pass particles, c) Dislocation loops occur and part of dislocation line is breaking off and moving on.

Another factor that causes the increased amount of dislocations is the different thermal expansion coefficient between the matrix and reinforcement particles in the composite [35]. The increased amount of dislocations is thought to occur during the transition from the temperature during production to room temperature [35]. Therefore, the strengthening can occur with mismatch CTE.

Finally, the load transfer by reinforcement is the transfer of the load to the rigid reinforcement through the metal matrix. According to R. Casati, the explanation of the load effect is that under an applied external force, the transfer of strain from the soft and compatible matrix to the stiff and hard particles contribute to the base material's strengthening [34].

2.1.4. Processing Methods of MMCS

The use of various matrices and reinforcements has led to the development of different techniques in the production of MMCs [36, 37]. In choosing the production method of composite materials; matrix, reinforcement, desired mechanical and physical properties and part shape are taken into consideration. The production methods of composite materials can be grouped under two main headings as solid-state production and liquid state production techniques.

In solid phase production methods, the chemical interaction between the matrix and the reinforcement are unlikely to happen. These methods aim to effectively mix the matrix powders with the reinforcement and obtain the samples by conventional powder metallurgy methods [36]. In addition to powder metallurgy, mechanical alloying, diffusion bonding and spark plasma sintering are also solid-state production methods [38]. The powder metallurgy method is frequently used among solid phase production methods [38].

It is known that the production of MMC materials by the liquid phase method is more economical and advantageous than the solid state, especially powder metallurgy method [39]. A liquid metal matrix can be incorporated or combined with the reinforcement to create MMCs. Using a liquid phase method in processing has a number of advantages [36]. These are near-net-shape component production, a faster processing speed compared to solid-state methods [36]. The most popular liquid phase production methods can be classified into three groups:

a. Casting and infiltration
b. Spray co-deposition
c. In-situ

These methods of the liquid phase will be explained briefly. Firstly, casting is the method of a liquid metal infiltrating a fiber or particle preform [36]. When short fibers or particles are directly introduced into a liquid combination containing molten metal, the mixture is frequently agitated to achieve a homogenous particle distribution [34]. Squeeze casting, also known as pressure infiltration, is the process based on infiltrating a fibrous or particle preform by molten metal using pressure [34]. This method is especially well adapted to complex-shaped components, localized or selective reinforcing, and high-speed production [13].

In spray co-deposition method, a particle injector puts ceramic particles into the spray stream, resulting in a granulated combination of composite particles [13]. After that, the composite particles are solidified using an appropriate technique such as hot-pressing, extrusion, and forging [38].

In-situ is a process of obtaining a two-phase composite microstructure in a controlled manner with reinforcement that is formed whereby precipitation due to the melt during cooling and solidifying [40].

In this study, the stir casting method, which is under the liquid phase production methods, is used for the fabrication of composites. Therefore, the stir casting method will be given in detail.

Stir Casting

Stir casting is often regarded as a very promising method for fabricating discontinuous MMCs and it is currently used commercially. Its advantages are its ease of use, adaptability, and suitability for large-scale production [41]. It is also appealing since, in general, it allows for the use of a traditional metal production approach, lowering the product's final cost [41]. This liquid metallurgy method is the most cost-effective MMC manufacturing option, and it allows for the fabrication of extremely large components [41].

The stir casting process begins with liquefying the metal, followed by various methods of inserting ceramic particles into the melt, and finally allowing the melt to solidify on its own or utilizing controlled solidification parameters [36, 37, 42].

In the literature, there are many studies on the stir casting method. Manoj Singla et al. [41] attempted to make aluminum-based silicon carbide particulate MMCs with the goal of developing a standard low-cost MMC manufacturing technology and achieving homogenous ceramic material dispersion. Their research obtained that increased hardness and impact strength have been perceived with an increase in SiC content. In the samples created with manual mixing, and using the 2-Step technique of stir casting method, homogeneous dispersion of SiC particles in the Al matrix exhibits a rising trend [41]. Afshin Matin et al. [43] produced SiC reinforced AZ80 and Mg nanocomposites with stir casting technique for improving the microstructure and room temperature mechanical properties of SiC reinforced AZ80 and Mg nanocomposites. They reported that it became more difficult to achieve homogeneity with increasing SiC addition.

Khalid Mahmood Ghauri et al.[44] have reinforced pure aluminum with various ratios of SiC (particle size less than 10μm) by casting method. They used manual mixing method while adding the reinforcement and then mechanical mixing method when the desired temperature was reached. The results revealed some problems such as poor particle distribution, lack of uniformity, coexistence of particles, and absence of particles in some places in the samples obtained by manual mixing [44].

Palash Poddar et al. [45] used a stir casting to manufacture SiC reinforced Mg and its alloy (AZ91D) matrix composites and examine their mechanical and microstructural qualities. The results show that the stir casting operation at 680°C led to successful production of reinforced magnesium-based MMCs with minimum porosity (close to theorical density). The homogeneous dispersion of SiC particles and the good interface obtained between SiC reinforcement and matrix demonstrated the applicability of the current processing technology [45].

J. Hashmi et al. [46] assessed the comparatively low-cost mixed casting method for the production of MMCs, as well as presenting and discussing the technical issues encountered. In that research, it was possible to obtain a composite with a wide range of mechanical properties, subject to the satisfactory result of the presented distribution of reinforcement, wettability, and porosity [46]. It is suggested that principal points to be emphasized in MMC materials prepared by mixing casting procedures are as follows [36, 37, 47]:

- The difficulty of homogeneous distribution of reinforcement
- Wettability between matrix and reinforcement
- Porosity in cast MMCs
- It can be listed as the chemical reactions between matrix and reinforcement.

The reinforcement must be distributed uniformly in the matrix and the wettability between them must be considered in order to obtain effective incorporation of reinforcement in the resulting composite material [37].

When adding nano-sized reinforcement into molten metals by the stir casting, agglomeration of particles, and porosity is seen due to gas retention, hydrogen formation, and shrinking during solidifying [48]. Therefore, it reduces the mechanical properties of MMCs. Even when mechanical mixing is added to the melt before casting, significant agglomeration of nanoparticles happens frequently in composites made by the traditional liquid metallurgical process [48]. This is due to the high surface-to-volume ratio of the nano-

sized ceramic particles, which causes high viscosity and poor wettability in the molten metal [11]. This can be overcome by applying ultrasonic mixing in the manufacture of MMCs. Figure 2.5 shows the distribution in molten metal using an ultrasonic stirrer schematically for MMCs production.

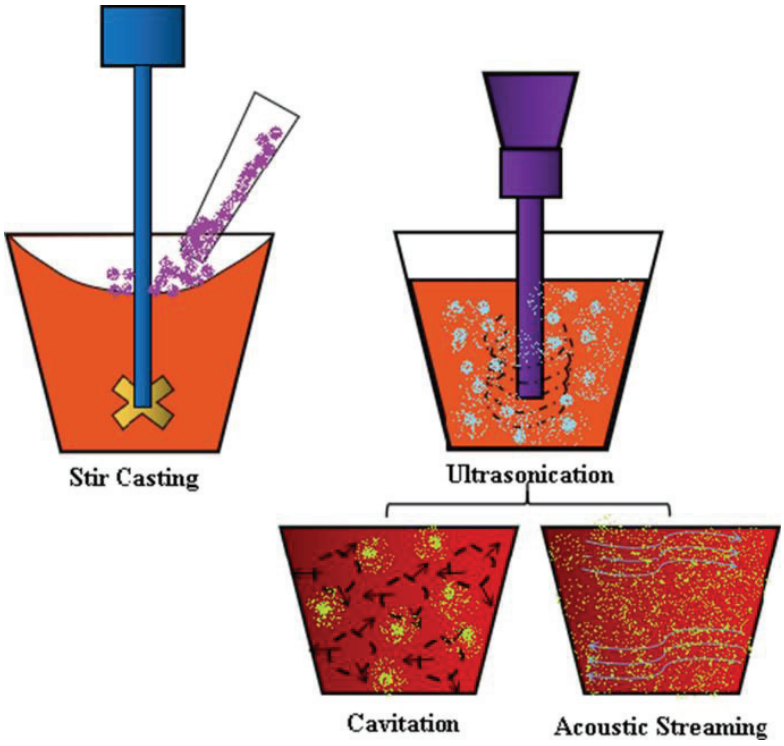

Figure 2.5. Schematic view of stir casting process and ultrasonic stir [49].

Liquid metal with a more homogeneous inclusion distribution is obtained compared to other methods with ultrasonic vibration [37]. Thanks to the cavitation bubbles formed during ultrasonic mixing, the hydrogen gases in the liquid metal are removed, while the oxide films in the liquid metal are broken and dispersed homogeneously [42].
In the literature, there are studies on MMC materials that show the effect of an ultrasonic stir. Amir Hussain Idrisi and Abdel-Hamid Ismail Mourad obtained samples that have different contents of SiC reinforcement into the aluminum alloy (AA5083) using an ultrasonic stir and without an ultrasonic stir for evaluating the influence of ultrasonic procedure [50]. In their microstructural examination, it has come into view that microparticles of SiC were homogenously distributed in the matrix when an ultrasonic

mixer was utilized. In addition, in the test results, they noticed that the mechanical and physical properties were enhanced by the ultrasonic-assisted stirred casting process [50]. A. Khandelwal et al. [51] studied how ultrasound helped solidify AZ31/Al_2O_3 metal matrix nanocomposites and how that affected their mechanical properties. After ultrasonic-assisted mixed casting, their microstructural investigations revealed a reasonably equal dispersion of Al_2O_3 nanoparticles in the Mg matrix [51]. K.B. Nie et al. [52] produced SiCp reinforced AZ91 composites by ultrasonic vibratory stir casting method and experimentally investigated the tensile and microstructure properties of the composites. They observed that accumulates of SiC nanoparticles throughout the grain boundaries clearly grow as the volume fraction of SiCp accrued [52].

Wettability

Wettability is an assessment of an interfacial pulling of liquid and solid to another liquid or solid [11]. It is a force balance between adhesive and cohesive intermolecular interactions that govern an inclination of liquid to sustain contact with the surface of a solid material. Contact angle of a liquid drop on solid with the solid surface (θ) is a physical measure of wettability. Contact angle can be determined using test methods such as sessile drop. Accordingly, Figure 2.6 shows the wettability of materials based on the contact angle. The angle of contact between a drop of liquid lying on a solid substrate can be used to represent wettability. The following equation, often known as the Young–Dupre equation, determines the contact angle at equilibrium [53] ;

$$\gamma_{sv} = \gamma_{sl} + \gamma_{lv} \cos\theta \tag{2.2}$$

where γ_{sv} is the solid-vapor specific energy of interface, γ_{lv} the liquid-vapor specific energy of interface, and γ_{sl} the liquid-solid specific energy of interface. It creates a liquid–solid and a liquid-vapor interface in place of a portion of the solid–vapor interface when a drop of liquid is set on a solid substance [53]. If the free energy of the system decreases, the spreading of liquid will occur. The work of adhesion, W_a, the bonding force between the solid and liquid phases is defined as seen 2.4 equation;

$$W_a = \gamma_{lv} + \gamma_{sv} - \gamma_{sl} \tag{2.3}$$

$$W_a = \gamma_{lv}(1 + \cos\theta) \tag{2.4}$$

For that reason, the contact angle and surface tension of the liquid can be used to express the bonding force between the liquid and solid phases [53]. The wettability will be described by the magnitude of the contact angle. When contact angle is equal to zero (0), wettability occurs [53]. If contact angle is between the 0 and 180, the wettability of system is not sufficient, i.e., Partial wetting [53]. However, if contact angle is equal to 180, there is no wettability.

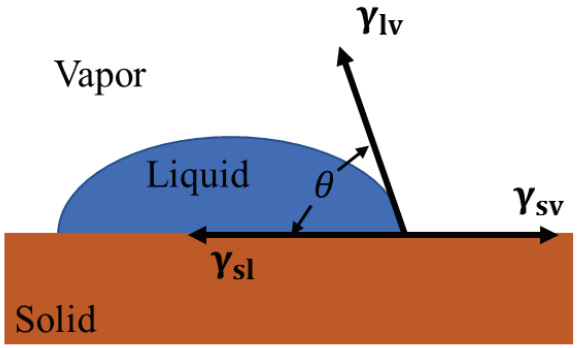

Figure 2.6. The surface wettability based on the contact angle (θ).

Wettability depends on many parameters such as interface chemical reactions, process temperature, time, atmosphere, porosity and roughness of reinforcement, and can be affected by many factors [53]. The existence of an oxide layer on the molten metal surface has a negative effect on wetting because it prevents particle reinforcements from penetrating the liquid metal [53]. Furthermore, ceramic particle surfaces are commonly covered with gas, which reduces wettability by preventing molten matrix material from contacting the ceramic surface. Particle surface characteristic is another factor that affects wetting [53]. The impurities absorbed on the particle surface can reduce wettability [53].

The addition of alloying elements into the matrix alloy, ceramic particles coating by a readily wettable ingredient, and processes applied on ceramic particles are the main solutions used to improve wettability [6]. As an example, a multitude of materials with various wetting conditions have been produced and used to reinforce MMCs and metal matrix nanocomposites; nevertheless, the wetting properties of these nanomaterials remain a challenge in all composite manufacturing procedures [6, 11].

2.2. Wear

Wear is a progressive deterioration that results in material loss due to excessive or prolonged use of the material [54]. As a result of wear, the shape and function of the part decline and/or deteriorate. The consequences for the user are as follows:

- Reduced working life and poor quality / decrease in production
- High energy consumption and low efficiency
- Increased job security risk for employees

Combined, these factors can result in significant costs. Therefore, the effects of wear on material life must be taken into account. Wear damages machines and surfaces. Changes occur as a result of wear on machine surfaces and metal hard surfaces [55]. Wear is a subject of Tribology. The study of interacting surfaces and the effect of this interaction on friction and wear is called "Tribology" [2, 54]. Three elements must be understood in order to provide the best possible characterization of wear mechanisms in metals:

1) Chemical composition, manufacturing process (such as rolled, forged, cast), and mechanical qualities are used to classify the base material. Also, one of the fundamental roles is the geometry of the part in this classification [56]. This classification identifies the material wear resistance, as well as the welding conditions required during repair, part restoration, and/or hard facing.
2) Abrasiveness causes the base material abrasion and it is qualified as its dynamic and physical features [56]. The hardness, form, and texture of the abrasive affect determine the level of damage it will cause based on the pressure it produces, its speed, and the angle at which it makes contact with the base material [56].
3) The environment in which the formation of wear is a significant detail in selecting the best welding solution [56]. Pressure, humidity, and temperature should all be characterized to the greatest extent possible [56].

Material loss on solid surfaces in contact can happen in three ways. These are chemical dissolution, local melting, and physical separation from the surface [2]. In practice, within the scope of wear, the damages determined by the material that is physically detached from the surface are involved. In a wear system; base material (wearing), counter material (abrasive), intermediate material, load and movement constitute the basic elements of wear [2]. The most frequently addressed wear mechanisms [2] in literature are given in Figure 2.7. An explanation of these four wear mechanisms is given below.

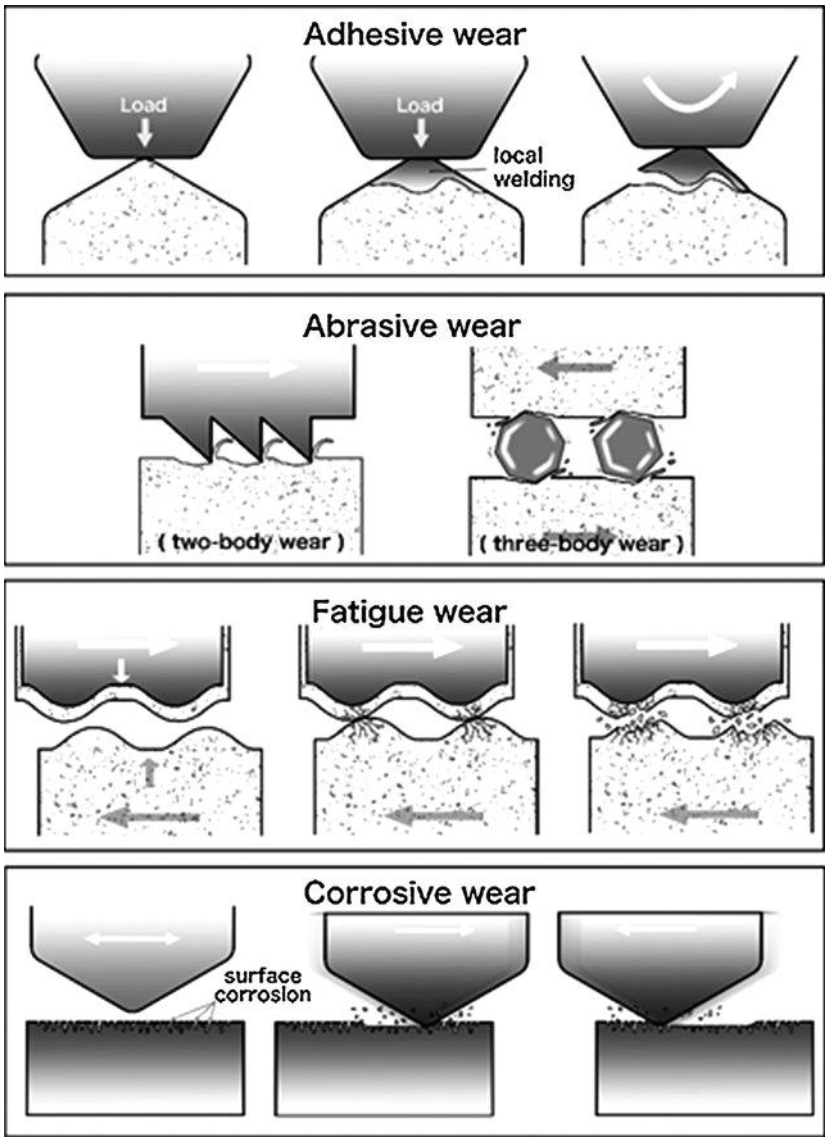

Figure 2.7. Schematic drawings of wear mechanisms [2].

Adhesive wear

The stresses on the surfaces sliding on each other reach or exceed the yield stress limit even with small loads. The adhesion forces between the metals in contact show themselves. Therefore, material transfer from one part to another, cold welding, and breaking off small parts occur [57]. Although adhesive wear is the most common type of wear, it usually does not accelerate the damage [2]. Adhesive wear takes place as a consequence of the breaking of asperities on the fused or adhered surfaces during the

relevant movement of a metal surface against another metal surface [2]. If the two metals are of the same hardness, wear occurs on both surfaces. Excellent lubrication between metals, reducing the load acting on the surface, and increasing the hardness of the material reduce adhesive wear [58]. As a result, adhesive wear is proportional to the normal load acting on the surface, the sliding path, and the surface hardness of the wearing material.

Abrasive Wear

Abrasive wear is the event of chip removal at the micron level by scratching the other material by the roughness peaks or grains of the harder of the two materials in contact with the effect of the applied load and movement [2]. Abrasive wear occurs during sliding when metal surfaces, one of which is harder and rougher than the other, are in contact with each other [58]. Penetration of hard particles into the soft metal can cause abrasive wear [2]. An example of this mechanism is the wearing style caused by dust particles entering the system from the outside or combustion products that are formed in an engine [58]. The abrasive wear rate can be reduced by reducing the load acting on the material surface. Thus, it is ensured that the particles sink less into the surface and leave less traces during deburring.

If the abrasive material is between two metals in free form, or if there are fixed or free grains that abrade only one metal, in this case; two-element abrasive wear and three-element abrasive wear, grouping is possible [2]. In metal-to-metal friction, wear begins as a two-element abrasive or adhesive and continues as a three-element abrasive [2]. In this case, the intervening dust, mineral grains, microchips released as a result of scratching and fragmented oxide particles can form the third element which is intermediate material [2]. Since the released microchip particles are generally harder than the base material (three-element), abrasive wear accelerates [2].

Fatigue Wear

It is a type of wear that occurs mostly due to the fatigue of the internal structure under or near the contact surface as a result of dynamic stress and the breaking off small parts from the surface [2]. Natural hardness is an important consideration in this type of wear. Fatigue wear is not seen in soft materials [2].

Corrosive Wear

The chemical and electrochemical destruction of contact surfaces is called corrosion. Various layers are formed in the surface structure as a result of chemical, electrochemical and metallurgical relations between metal and its alloys and their environment [2]. The removal of the layers on these rubbing surfaces by breaking them is called corrosive wear.

Types of Wear Test

It is possible to classify the wear tests, which are caused by the movement of solid materials with each other, with three wear tests. The positions of the samples are different in the types of wear test.

Pin-on-disc

Usually, the sample is secured by a holder and placed on the disc. The force is applied through the holder. The weight (load) is placed on the sample. Generally, the sample is elongated cylindrical in structure. The sample surface should be parallel to the disc. The disc rotates and wears on the sample over time, or the disc remains stationary. The pin (sample) moves forward and backward in parallel movement. Figure 2.8 shows the schematic of pin on wear tests pictures.

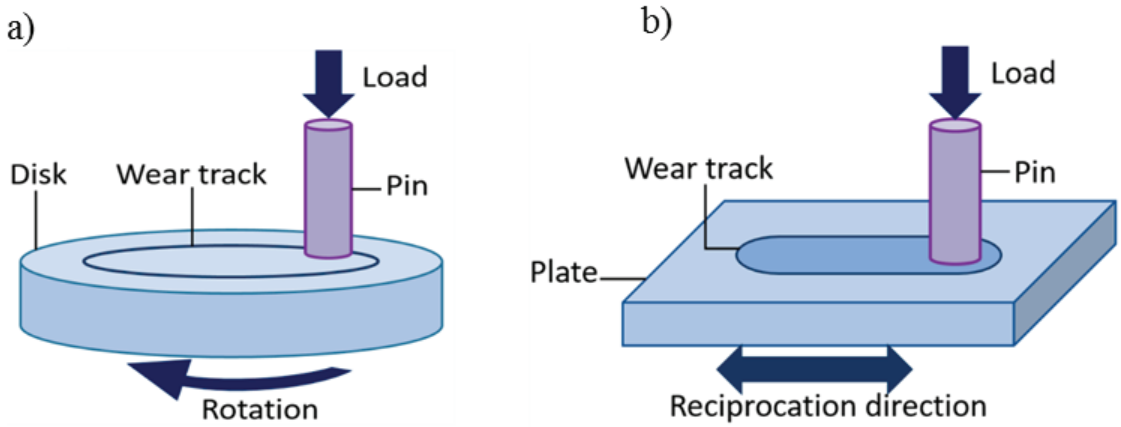

Figure 2.8. Schematic of a) pin-on-disc test and b) pin-on-plate test [59].

Ball-on disc

The sample is placed on the disc. The diameter of the sample is larger than the samples used in pin-on-disc test. At the same time, the sample does not need to have a circular surface. It is sufficient to have a shape that can be attached to the holder and a surface area where the ball of the desired diameter can be found. After a sample is placed on the disc, the ball is put on the sample in the desired diameter with the ball holder. Wear marks can be seen on the sample over time with the rotation of the disc. The disc remains stationary. The ball moves forward and backward parallel with the shape. Figure 2.9 shows the schematic of ball on sliding tests. In this study, the ball-on-disc test was performed. The test conditions for the ball-on disc test are indicated in the experimental procedure section.

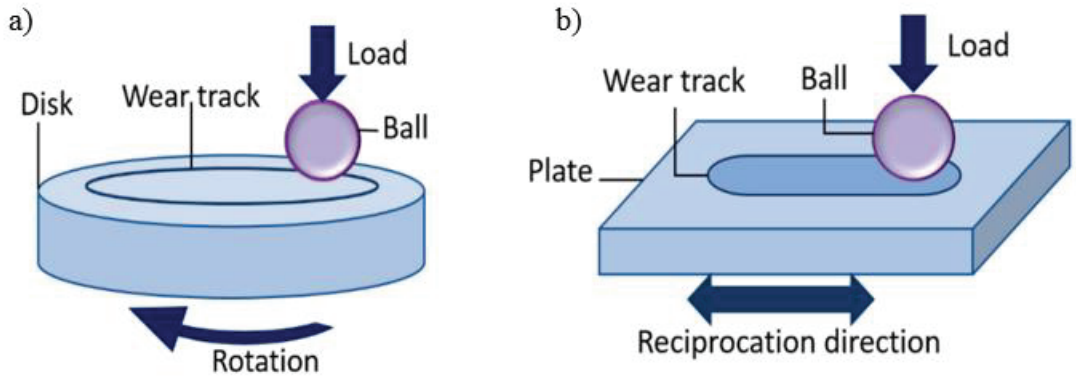

Figure 2.9. Schematic of a) ball-on-disc test, b) ball-on-plate test [59].

Three-body wear

In the three-body wear test device, the sample and disc are positioned as shown in Figure 2.10. Fine-grained sand is sent between the sample and the surface during the test. In the case of three-body abrasion, particles can slide and roll among mating surfaces.

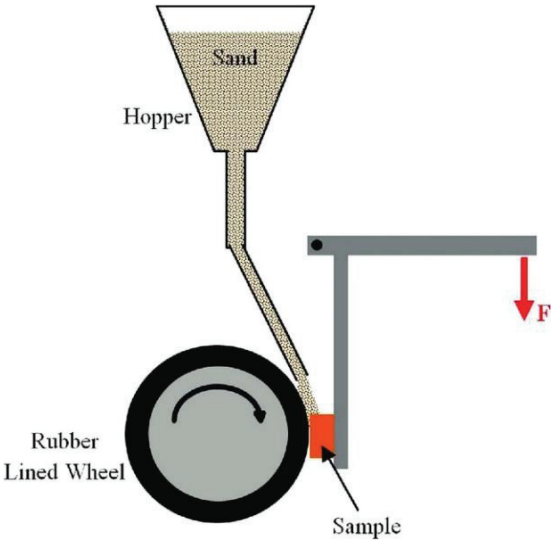

Figure 2.10. Three body wear test [60, 61].

Another important characteristic considered in the determination of the wear behaviors of MMCs other than the wear resistance is the friction coefficient. In the most general sense, the friction coefficient is defined as the ratio of friction force to load. The main factors affecting friction under dry sliding conditions in MMCs are adhesion of flat areas on the rubbing surfaces, scratching carried out by the abrasive particles and hard surface roughness, and deformation of the surface roughness. The effect of such elements on the friction coefficient value depends on friction conditions and the environment.

Kavimani V. et al. [62] investigated the impact of reduced graphene oxide (r-GO) nanosheets on the dry sliding wear behavior of AZ31 based composites manufactured using a solvent-based powder metallurgy method. In their research, the pin-on-disc tribometer for an optimal set of control factors was used for the tribological behavior of composites. As input parameters, they employed the percentage of reinforcement weight, sliding distance, load, and sliding velocity. The results of the study demonstrated that reinforcement weight percentage and load have the greatest influence on the specific wear rate.

Liqun Wu et al. [26] added nickel-coated GNPs as reinforcement into AZ31 Mg alloy. In their wear test results, they indicated that the essential factor of the low wear and COF obtained in composites compared to the reference AZ31 alloy is the effect of GNPs. They also remarked that the type of wear mechanism is abrasive wear [26].

Juanjuan Zhu et al.[63] investigated the role of SiC and WS2 in improving the mechanical strength of Mg MMCs (pure Mg and AZ31 Mg alloy) by ball-on-disc wear tests at room temperature (RT) and 110 °C. The composites were obtained by spark plasma sintering. They observed that the adhesion mechanism occurred in wear tests performed at 110 °C in Mg MMCs. They noticed that COF of Mg MMCs were decreased by 37.5% and 54.5%, respectively. In addition, the wear resistance of Mg composites is more favorable than unreinforced Mg and AZ31 Mg alloy in all test conditions [63].

M.Arab and S.P.H.Marashi investigated the mechanical and tribological properties of AZ31 Mg matrix composite by adding various contents of GNP [31]. In the research, the composites were obtained with friction stir processing. Their results of pin-on-disc tests show that COF was reduced 25–45% compared to unreinforced AZ31 in GNPs reinforced AZ31 composites [31].

2.3. Motivation of Thesis

There are researches to increase the use of MMCs in the literature [9, 64, 65]. The studies are at the forefront of expanding the use area of light metals that have been popular lately in research on MMCs [4, 5, 8, 66]. Some opinions suggest that Mg can be a preferred study because of its lightness and suitability for mass production [67, 68]. Several types of research about Mg and its alloy composites have been well documented. The investigations on the Mg alloys AZ91 and AZ31 appear to be more than investigations on the ZE10 Mg alloy [31, 51, 62, 67, 69, 70]. SiC has more studies as a reinforcement than graphene in MMCs [7, 43, 53, 66, 71]. The growing research and application fields of graphene are attracting attention [7, 20]. In addition, many studies were suggested that graphene can play an active role in improving magnesium properties [3, 7, 12, 30, 72]. The limited number of graphene reinforced Mg matrix composite studies is one of the motivations of this study [8, 13, 70]. Another is that few studies of graphene nanoplatelet reinforced Mg MMC produced using the liquid phase casting method, which is one of the manufacturing methods [46]. The few studies on the ZE10 alloy and the fact that the studies related to GNP reinforced ZE10 matrix composites have not been published yet influenced the creation of this study [65, 71, 73, 74]. In addition, another motivation of the study is to contribute research on wear and hardness measurements at various temperatures in GNP reinforced Mg matrix composites. In summary, the objective of this research is to contribute to literature by fabricating GNP reinforced ZE10 alloy MMCs in the liquid phase and investigating wear and hardness tests at various temperatures.

CHAPTER 3

EXPERIMENTAL PROCEDURE

3.1. Materials

ZE10 magnesium alloy was selected as the matrix material and GNP was selected as the reinforcement in this study. The chemical composition of ZE10 magnesium alloy including rare earth elements [71] is given in Table 3.1. The existence of the rare earth element in the alloy is known to provide improved formability, ductility, creep, and corrosion resistance [75]. Graphene is important reinforcement because graphene has extraordinary thermal, mechanical, and electrical conductivity properties [20]. The dimensions of GNPs used, are approximately 10-20 nm thick, 14 μm in diameter and their purity is 99%.

Table 3.1. Chemical composition of ZE10 alloy.

Composition (%)	Al	Zn	Mn	Mn	Nd	Ce	La	Zr
ZE10	<0,010	1,37	0,017	1,37	0,0079	0,28	0,23	0,065

3.2 Composites Fabrication

Casting was used for obtaining composites. In the first step, approximately 1.5 kg of Mg alloy was melted in steel mold using an electrical resistance furnace. When the temperature reached to 700 °C, mechanical mixing was applied with a steel stirrer at 1000 rpm for 5 minutes. During, the mechanical mixing process GNPs were added into the molten metal. In order to distribute the GNPs homogeneously and prevent agglomeration, the mechanical stirring was followed by ultrasonic processing with a UIP 1500hd Hielscher sonicator for another 5 minutes. The amplitude of titanium probe was set to 30 μm. The whole composite casting was performed under Ar/1% SF_6 shielding gas. After

the distribution process was completed, the steel mold containing the liquid composite was held in a water tank for solidification. The dimensions of the mold are 11 cm diameter, 15 cm long. The schematic image of GNP-reinforced magnesium matrix nanocomposites production by casting is shown in Figure 3.1.

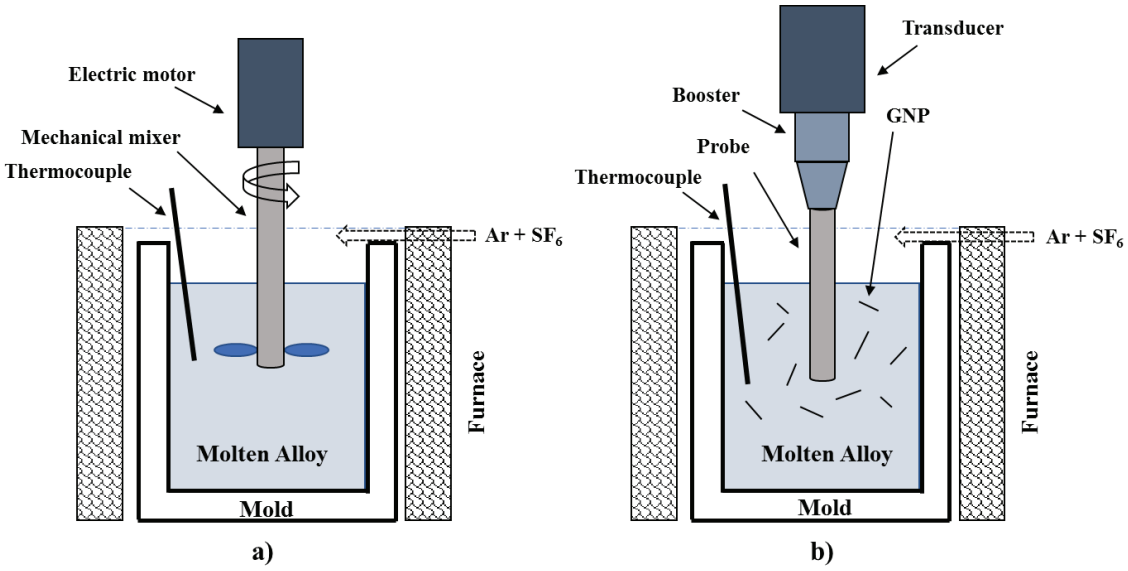

Figure 3.1. Schematic image of GNP-reinforced magnesium matrix nanocomposites production by casting a) Mechanical mixing of the alloy, b) Ultrasonic mixing and GNPs in the molten alloy.

GNPs were incorporated into the matrix with different mass ratios, i.e., 0.25 wt.%, 0.5 wt.%, and 1.0 wt.%. In addition, unreinforced ZE10 alloy (0 wt.% GNP) was also cast under the same processing parameters for comparison.

In order to carry out the wear tests and microstructural characterization of the produced composites, samples were obtained 15 mm diameter and 7 mm height. In addition, the surfaces were ground with 320, 600, 1200, and 2500 grit sandpaper, respectively.

Principle of Archimedes was used to quantify the bulk density of composites using Mettler Toledo ME204 balance with 0.1 mg precision in pure water as the immersion water medium. The porosity content in the samples was calculated using equation 3.1 [76].

$$P = \left(\frac{1-\rho}{\rho_o}\right) * 100 \qquad (3.1)$$

where, ρ is experimental density (Archimedes' principle) and ρ_o is the theoretical density.

In this study, the average grain sizes were found using the intercept method. Through the micrograph, a straight line is drawn in this technique. It is counted how many grain boundaries meet the line [77]. The average grain size is calculated by dividing the number of concurrences by the actual line length [77]. In this study, the ImageJ program was used for this technique. Ten lines were drawn and average grain size calculated for each composite micrograph.

3.3. Microstructural Characterization

The examination of reference alloy and nanocomposites were conducted by optical microscope, scanning electron microscopy (SEM), X-Ray diffraction (XRD), and 3D profilometer. The details of these devices are given in the following sections.

3.3.1. Optical Microscopy

Optical microscope is a system that magnifies images of small specimens using a lens system and visible light so that microstructural features such as grains can be visible. The microstructural examination of the samples in this study, before the wear tests, was performed by means of (a Leica DMI5000) model optical microscope which is shown in Figure 3.2.

Figure 3.2. Leica DMI5000 model optical microscope is used for examining the samples.

3.3.2. Scanning Electron Microscope (SEM)

The morphology and microstructure of materials can be investigated at higher magnification with SEM. SEM utilizes electrons which interact with atoms on the sample surface and produce different signals. These signals provide the information about the sample to be displayed on a computer screen. Two different SEM devices were used for examining the samples in this study. One of them is the FEI Quanta FEG 250 model SEM device, used before the wear tests. After the ball-on-disc tests, the worn surfaces of samples were analyzed under, a Hitachi TM1000 model SEM which is available at Tallinn University of Technology. (Figure 3.3)

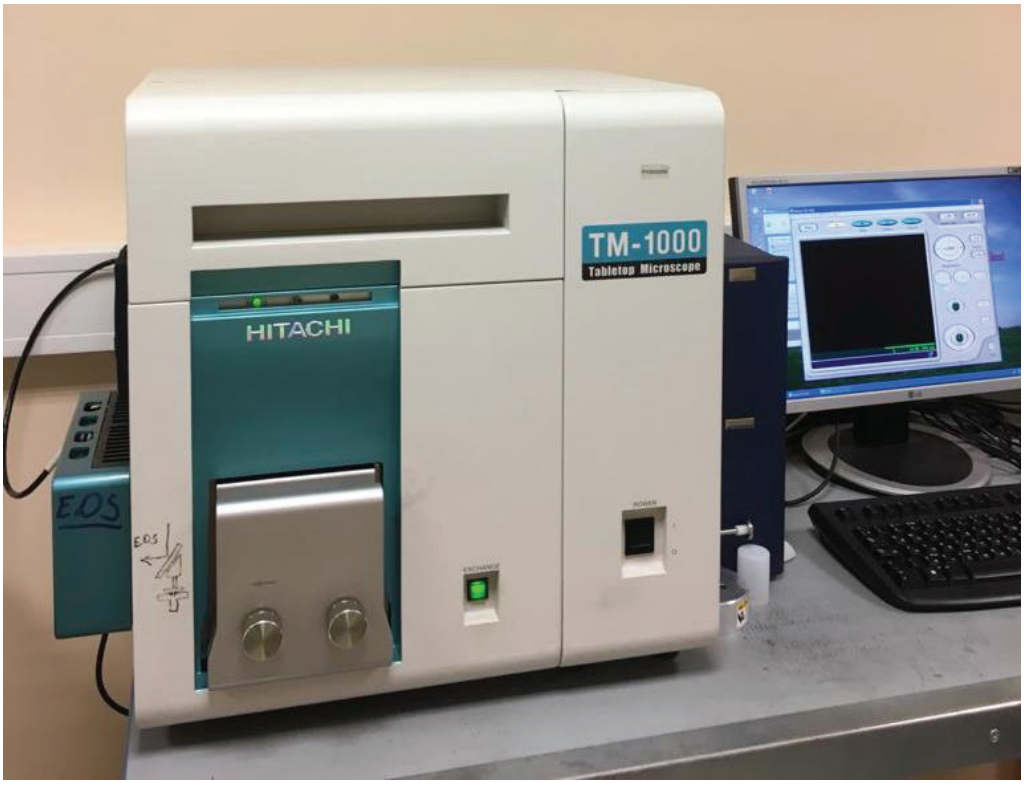

Figure 3.3. Hitachi TM1000 model SEM.

3.3.3. X-Ray Diffraction (XRD)

X-ray diffraction is a non-destructive technique for determining the phases they contain and the crystallographic characteristics of materials. The phase identification of samples was accomplished by using XRD equipment, Siemens Bruker D5005 X-ray analyzer with a Philips X'Pert PRO diffractometer, PANalytical, Netherlands. The following diffraction parameters were used: Cu K_α radiation (30 mA, 40 kV, $\lambda = 0.1542$ nm) in a $\theta - 2\theta^\circ$ scan with a step size of 0.02° and a count time of 0.4 s.

3.3.4. 3D Profilometer

After the wear test, samples have different volumes compared to their initial volumes. Potential differences in volumes need to be determined in order to better understand wear phenomena. In the literature, there are several methods for calculating

the volume loss. One of them is to calculate mass before and after test. Volume loss can then be calculated based on mass and density. Another method is to use a 3D profilometer after the ball on disc tests. In 3D profilometer, when light reaches to the surface of samples, it is reflected from the sample surface and tracks, and hence information about the surface topography is obtained. In this study, a high-resolution Bruker Counter GT-K model 3D profilometer, which is shown in Figure 3.4, was used for calculating volume losses of samples.

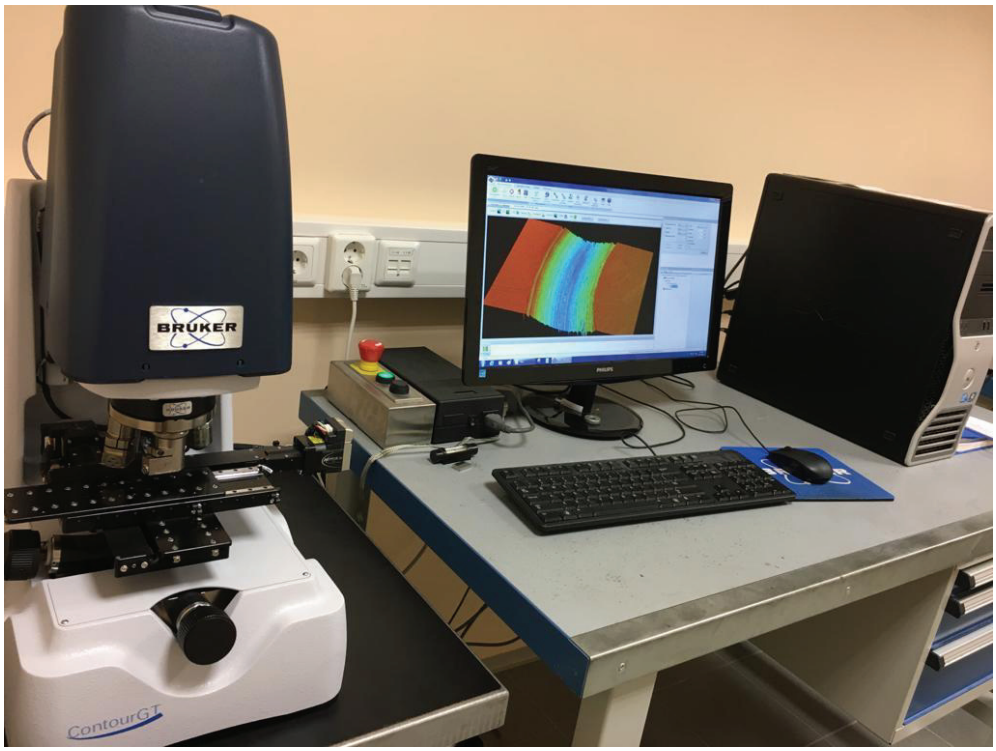

Figure 3.4. 3D profilometer for calculating the volume loss.

3.4. Mechanical Tests

In this section, the details of conducted hardness, wear, and tensile tests are given as follows.

3.4.1. Hardness

Vickers hardness test was accomplished at room temperature (RT), 100 °C, and 200 °C in order to measure the hardness values of samples at the temperature range in which the wear tests were applied. The Vickers hardness measurements were made by a CETR Bruker device which is seen in Figure 3.5. The indenter is Vickers HT Mitutoyo. The measurements were taken from four different points on a sample. Four indentations have 1,5 mm distance from the center and applying load is 3 kg. For each indentation, the sample was rotated 90°. Totally eight measurements were obtained for one set of materials and the average values were reported.

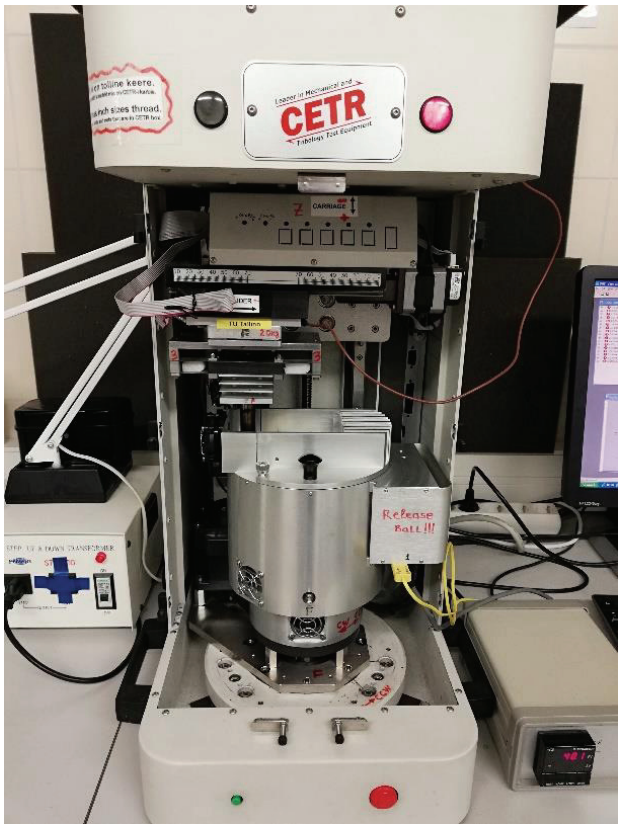

Figure 3. 5. Bruker CETR device used for hardness measurement.

3.4.2. Tensile Test

Tensile test is used to find out basic mechanical properties of materials such as strength. Tensile test involves pulling a test sample in one axis at a certain tensile speed and a fixed temperature until it breaks. During the test, specimens are elongated under applied force and all values are recorded. After tensile test, a strain-stress graph is obtained. A typical strain-stress graph for a ductile metal is shown in Figure 3.6. Yield stress, tensile stress, toughness, reduction in cross-section, elongation to failure, and elastic modulus of materials all can be calculated with tensile testing.

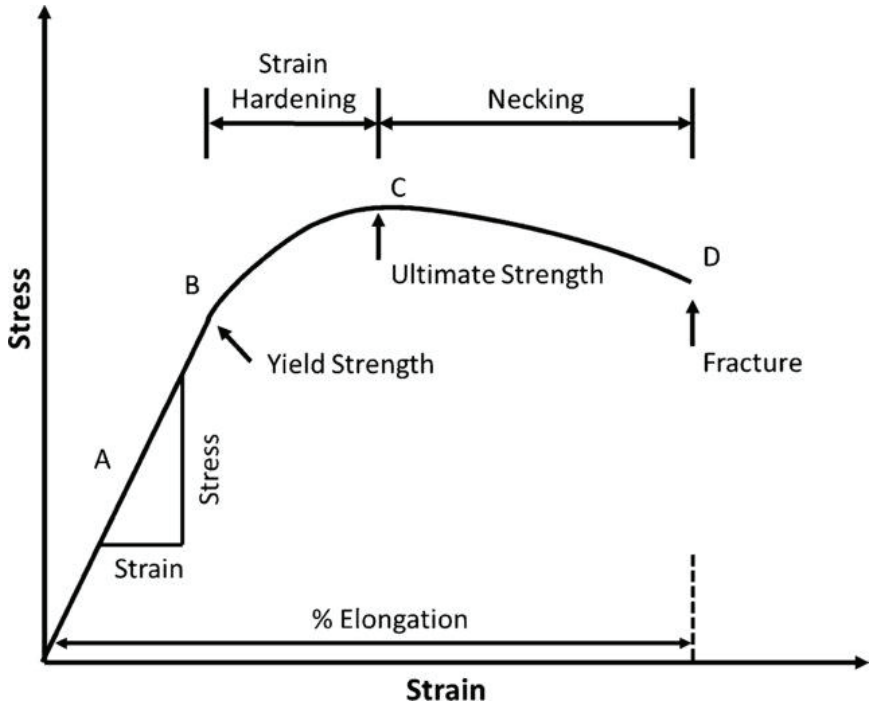

Figure 3.6. A typical strain-stress graph for a ductile metal [78].

In this study, the tensile tests were achieved using a Zwick Z050 testing device with a strain rate of 10^{-3} s^{-1} at room temperature. Five specimens were tested for each specimen and the average values were reported.

3.4.3. Wear Test

The wear behavior of the produced MMCs was investigated with the ball-on-disk test method to understand the effect of reinforcement contents on the wear resistance. The wear tests of the nanocomposite materials were performed in dry conditions with a CETR Bruker, UMT-2 model tribology device which is available at Tallinn University of Technology. One AISI 100Cr6 steel ball (62 HRC) in 10 mm diameter was used for each test in the ball-on-disc tests. During the ball-on-disc tests 2 N load was applied with a sliding speed of 0.1 m/s and 5 mm radius distance from center on the sample surface. In addition, the wear tests were carried out under the temperatures of RT, 100 $^{\circ}$C and 200 $^{\circ}$C. Prior to each test, the surfaces of the balls and samples were cleaned with acetone in order to prevent any contamination or external factors that may affect the test results. The wear test conditions are given in Table 3.2. A Bruker CETR device for ball-on-disc test and the parts of device are shown in Figure 3.7. The Hertzian initial contact value which is the maximum pressure between the ball and the sample surface was calculated to be 0,29 GPa. The wear amount values measured with 3D profilometer after the wear test and the coefficient of friction (COF) values were recorded. The acquired wear tracks were analyzed by SEM.

Table 3.2. Wear test conditions.

Steps	Load (N)	Duration (min.)	Speed(rpm)	Temperature ($^{\circ}$C)
Check Run	2	1	191	RT,100, and 200
Real Test	2	49	191	RT,100, and 200

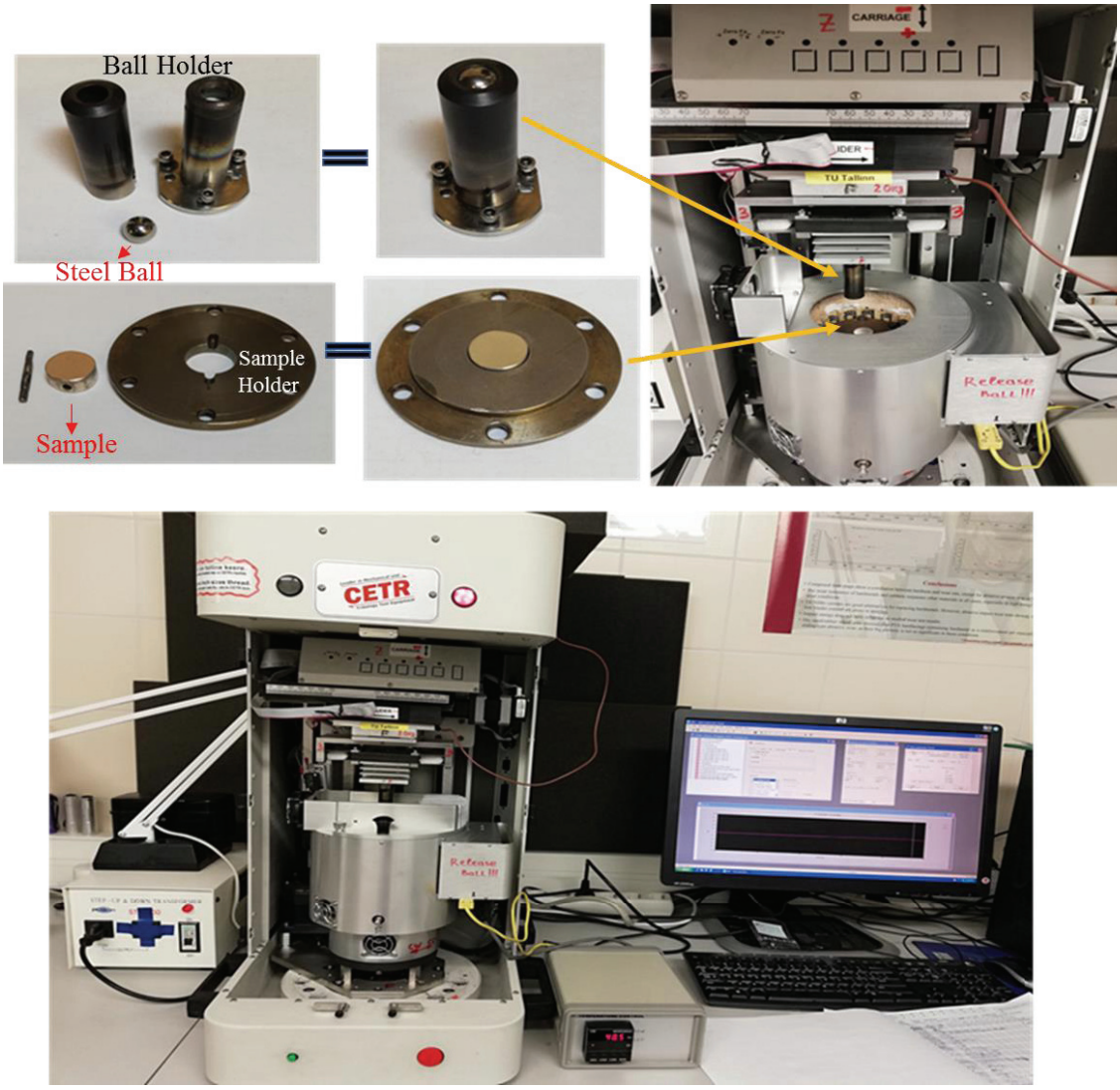

Figure 3.7. Bruker CETR device used for ball-on-disc tests and its parts.

CHAPTER 4

RESULT AND DISCUSSION

4.1. Microstructural characterizations

The results of the microstructural investigations are explained and discussed based on the order of processes in the following sections.

4.1.1. Optical Microscopy

Figures 4.1 and 4.2 compare the polarized optical micrographs and average grain sizes of unreinforced ZE10 alloy and ZE10 matrix nanocomposites. An increase in the grain size is seen with the added GNPs content. The average grain sizes of the ZE10 alloy, ZE10/0.25wt.%GNP, ZE10/0.5wt.%GNP, and ZE10/1.0wt.%GNP composites were determined to be 91, 144, 181, and 177 μm, respectively. This unusual grain coarsening by reinforcement addition in ZE10 alloy is consistent with an earlier study and the inactivation of Zr grain refining effect and the problems associated with the complement homogeneous reinforcement distribution [71]. In addition, the porosity ratio increases with increasing GNP content based on Figure 4.2. The increasing GNP content can lead to agglomerations in the composites. Therefore, the porosity could be increased. The agglomerations and porosity could be attributed to the inability of obtaining homogeneous distribution with the increased addition of nano-sized reinforcement.

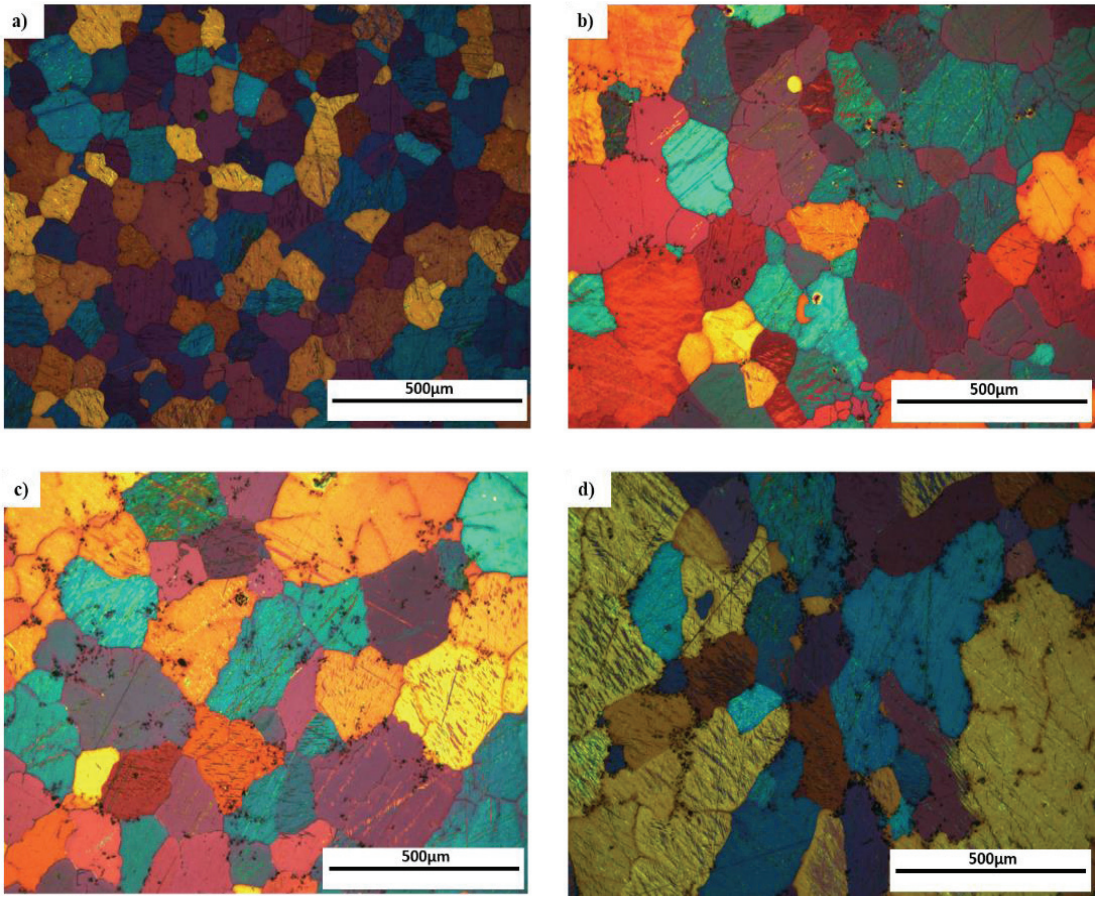

Figure 4.1. Optical micrographs of a) ZE10 Mg alloy, b) ZE10/0.25wt.%GNP, c) ZE10/0.5wt.%GNP, and d) ZE10/1.0wt.%GNP composites.

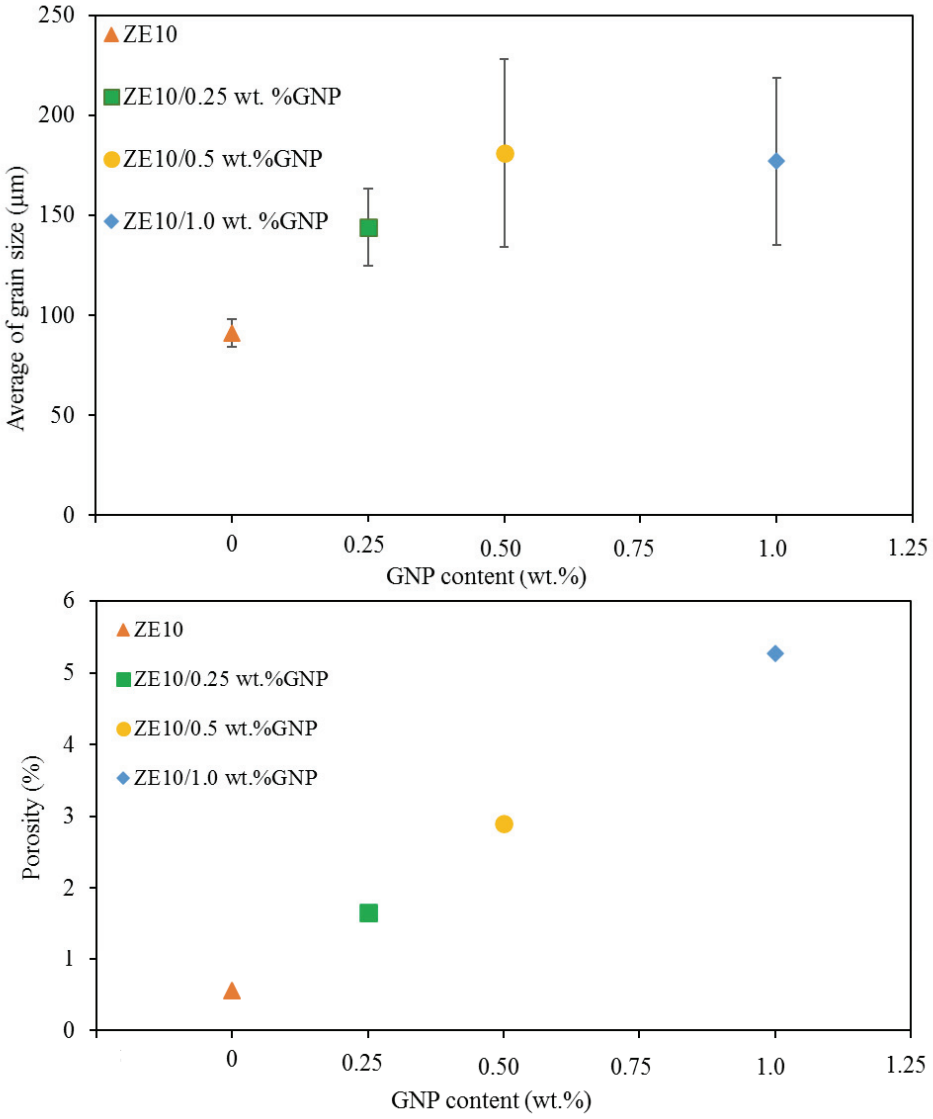

Figure 4.2. Average grain sizes and porosity rates of ZE10 alloy and ZE10 matrix nanocomposites.

Figure 4.3 shows the optical images of ZE10 alloy and ZE10 matrix composites at different magnifications. The micrographs of ZE10 alloy and its composites were analyzed. The grain coarsening can be seen at the region where graphene is absent (Figure 4.3). This grain coarsening can be ascribed to a location of GNPs and its content.

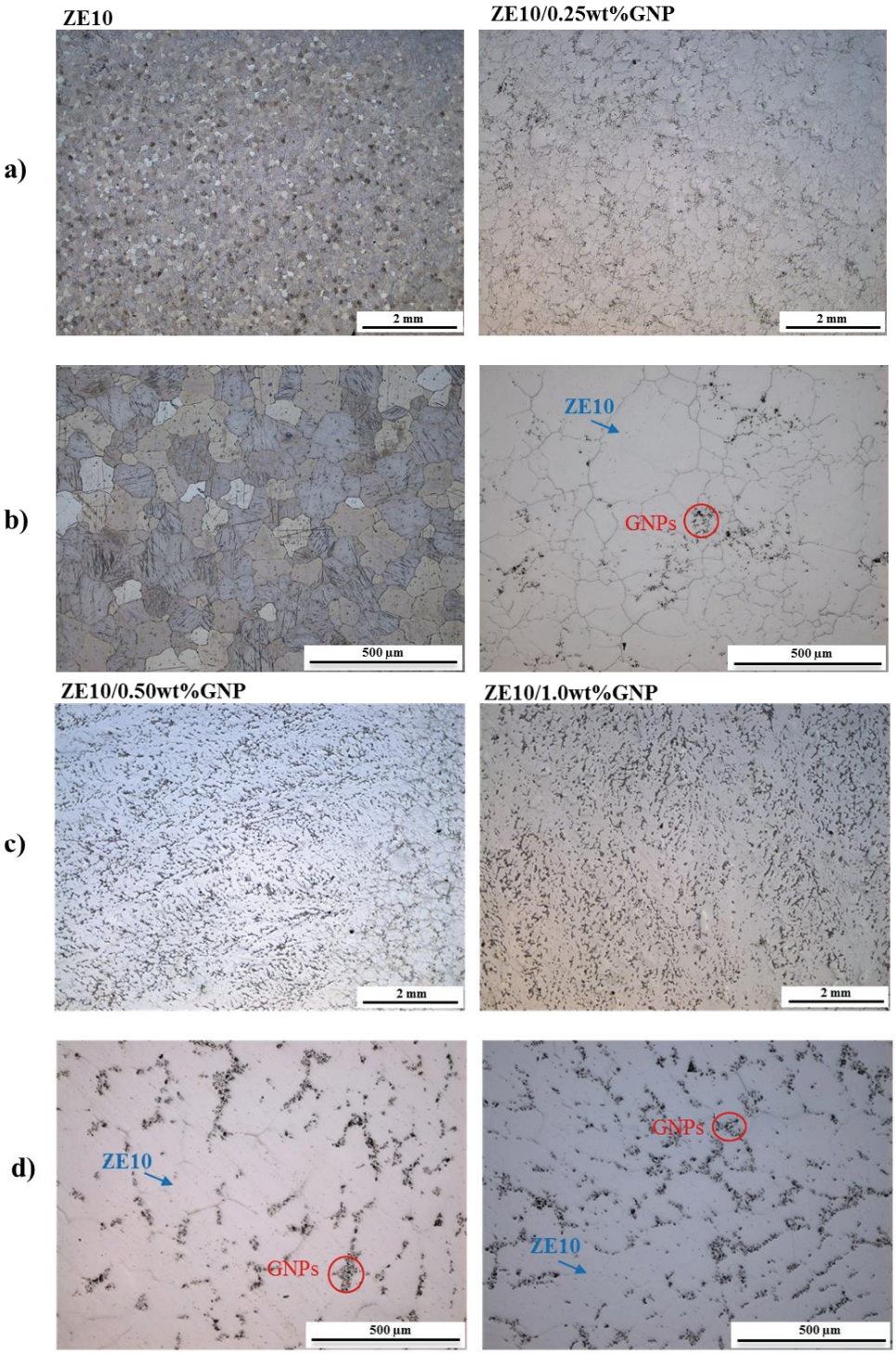

Figure 4.3. The optical images of a) the ZE10 alloy and ZE10/0.25wt.%GNP at 2 mm magnification, b) the ZE10 alloy and ZE10/0.25wt.%GNP at 500 µm magnification, c) the ZE10/0.5wt.%GNP and ZE10/1.0wt.%GNP at 2 mm magnification, d) the ZE10/0.5wt.%GNP and ZE10/1.0wt.%GNP at 500 µm magnification.

4.1.2. SEM Results

The SEM micrographs show some of the potential GNPs which were homogeneously distributed throughout the matrix as shown in Figure 4.4. It can be suggested that the mechanical stirring along with ultrasonic stirring applied during the composite fabrication process accomplished an influential role in the distribution of GNPs.

When the SEM micrographs are inspected, a certain amount of homogeneity is observed in the ZE10/0.25wt.%GNP and ZE10/0.50wt.%GNP composites for the reinforcement distribution. However, the SEM micrographs show that the addition of GNPs leads to agglomerations in the composites. The highest porosity rate was observed in the ZE10/1.0wt.%GNP composite (Figure 4.4). Homogeneous distribution became difficult and pores formation increased with the increase of GNP content. These results could be due to the surface energy of nano-sized reinforcement.

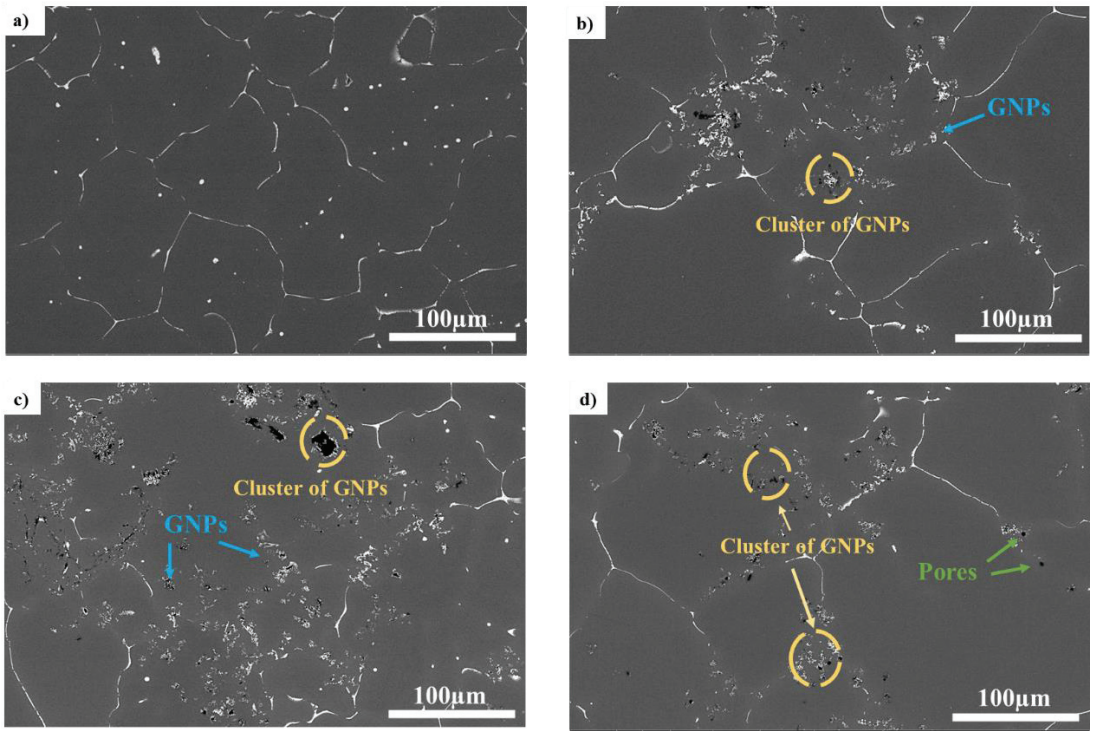

Figure 4.4. SEM micrographs of a) ZE10 Mg alloy, b) ZE10/0.25wt.%GNP, c) ZE10/0.5wt.%GNP, and d) ZE10/1.0wt.%GNP composites.

The energy dispersive X-ray (EDX) analysis in the SEM was utilized to ensure whether the potential homogeneously distributed particles were the GNPs. Figure 4.5 shows the EDX analysis of ZE10/0.25wt.%GNPs. As seen in the second spectrum result, the high carbon content indicates the locations containing GNPs embedded in the matrix.

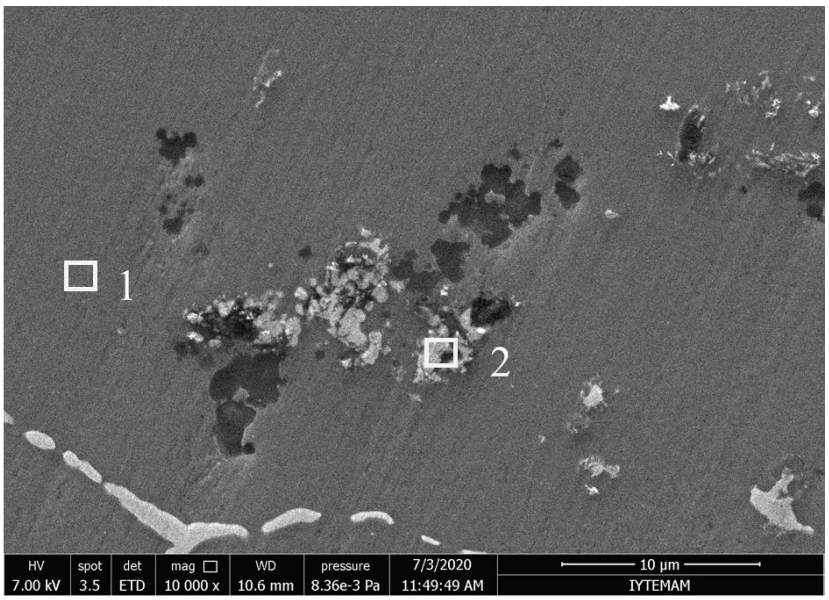

1 Spectrum

Element	wt.%	Atomic %
Mg	64.74	86.90
Zn	18.32	9.14
La	6.69	1.57
Ce	10.25	2.39
Total	100.00	100.00

2 Spectrum

Element	wt.%	Atomic %
C	84.63	92.93
O	5.44	4.49
Mg	3.41	1.85
Zn	1.11	0.22
Ce	5.41	0.51
Total	100.00	100.00

Figure 4. 5. EDX analysis for a grain region of the ZE10/0.25wt.%GNP composite.

4.1.3. XRD Results

Figure 4.6 shows the XRD analysis result and based on the literature research, GNPs show a single peak at approximately 26 degrees [19]. In the XRD results obtained, the peak is seen at 26 degrees. When looking at the peaks obtained as a result of XRD, the composites constituent α-Mg and the GNPs.

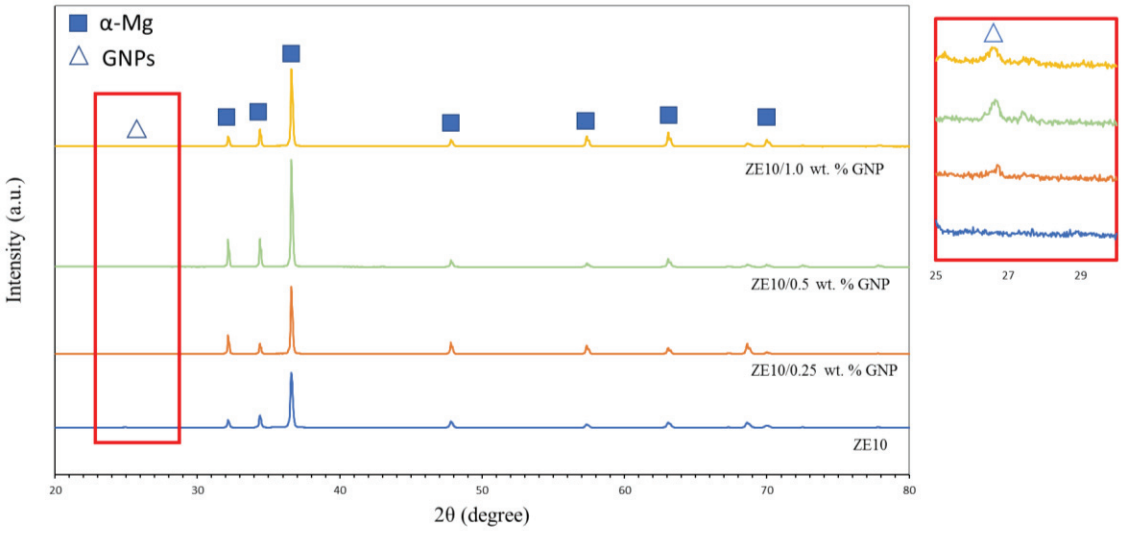

Figure 4.6. XRD analysis of the ZE10 alloy and its composites with the GNPs.

4.1.4. 3D Profilometer Results

The 3D profilometer images showing the depth and shape of the wear marks are given in Figures 4.7, 4.8, and 4.9. In these figures, the depths, and heights are revealed based on the color distributions. The measuring bar for each figure is given on the right side of the image.

When the ZE10 alloy and composites are examined, the lowest wear scar depth at RT is seen in the ZE10/0.25wt.%GNP composite. The ZE10/0.5wt.%GNP sample has the highest depth of wear scar than those of the ZE10/0.25wt.%GNP and ZE10/1.0wt.%GNP composites at RT.

When looking at the wear scars formed at 100 °C, the ZE10/0.25wt.%GNP composite has the improvement in the due to the least wear depth. The wear depth of the ZE10/0.5wt.%GNP composite is less than that of the ZE10 alloy. Therefore, the addition of GNPs may have led to less wear depth by increasing the hardness and strength. On the other hand, an increase is presented in the depth of the ZE10/1.0wt.%GNP composite. This could be due to the increasing tendency for agglomeration and porosity formation with increasing GNPs content.

The minimum wear depth is observed in the ZE10/0.25wt.%GNP composite when the wear scars formed at 200°C are examined. However, an increment in the distance

from the surface to the bottom of the wear scar is observed with the increase in temperature on the samples. The results indicate that the effect of GNPs on wear decreases with increasing temperature.

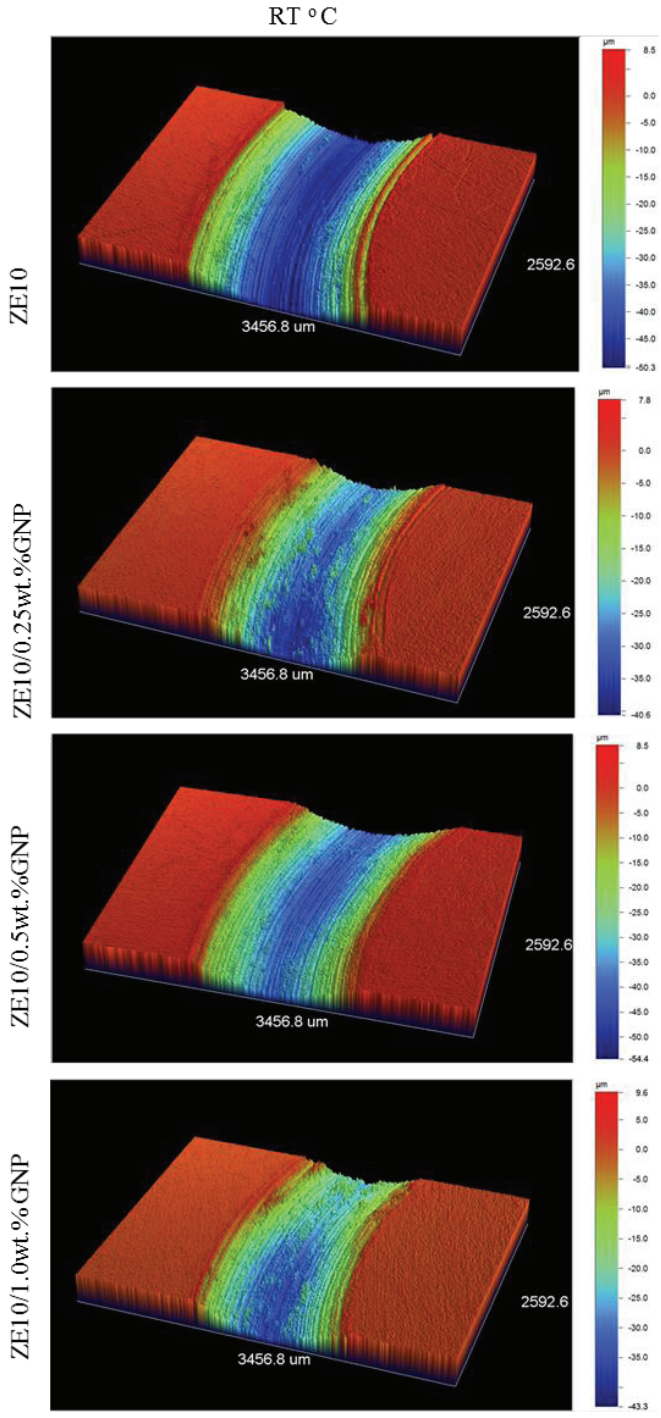

Figure 4.7. The 3D profilometer figures of ZE10 alloy and its composites with wear scar at RT.

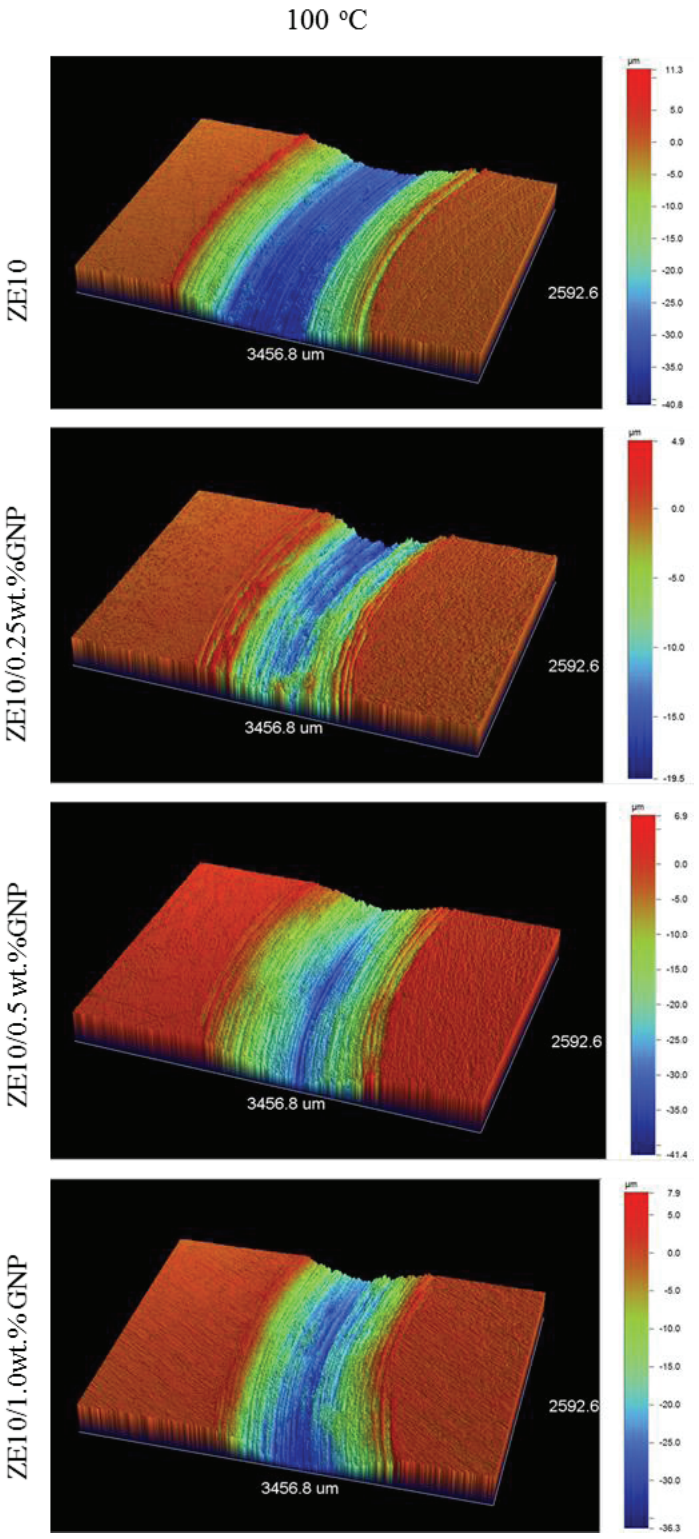

Figure 4.8. 3D profilometer images of ZE10 alloy and its composites with wear scar at 100 °C.

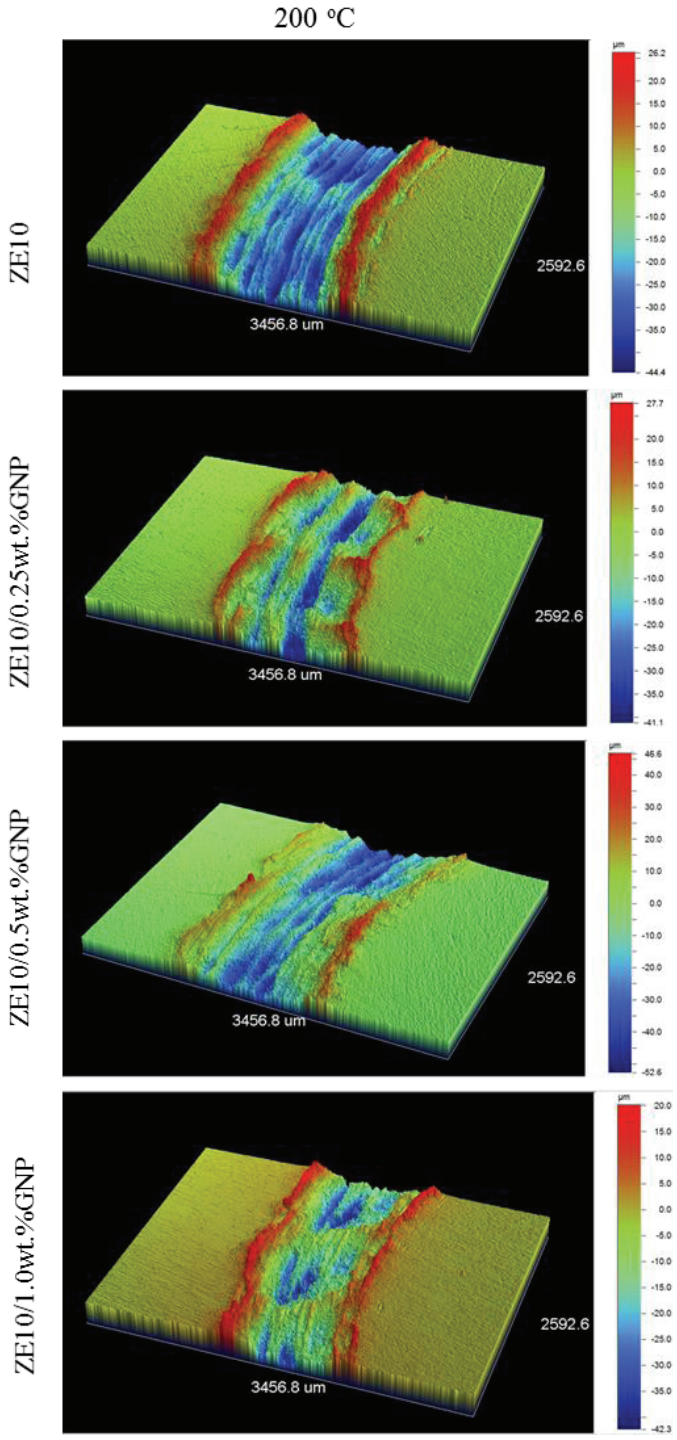

Figure 4.9. 3D profilometer images of ZE10 alloy and its composites with wear scar at 200 °C.

4.2. Mechanical Properties

In this section, hardness, wear, and tensile test results have been given, respectively.

4.2.1. Hardness Results

Figure 4.10 compares the average Vickers hardness values of ZE10 Mg alloy and its composites at RT, 100 °C, and 200 °C. The hardness at RT and 100 °C increases with the addition of GNPs compared to the unreinforced ZE10 alloy based on hardness test results. The hardness effect of GNPs is significantly dropped at 200 °C. The ZE10/1.0wt.%GNP composite has almost the same hardness value as the ZE10 alloy at 200 °C. In addition, the ZE10/0.25wt.%GNP composite has the greatest hardness value among other samples at 200 °C. The result suggests that the ideal GNP content is 0.25wt.% in terms of high temperature hardness properties. Considering the results GNPs reinforced nanocomposites showed better hardness performance than unreinforced alloy. The enhancement in hardness can be attributed to the reasonably dispersing of the GNPs into the ZE10 alloy matrix.

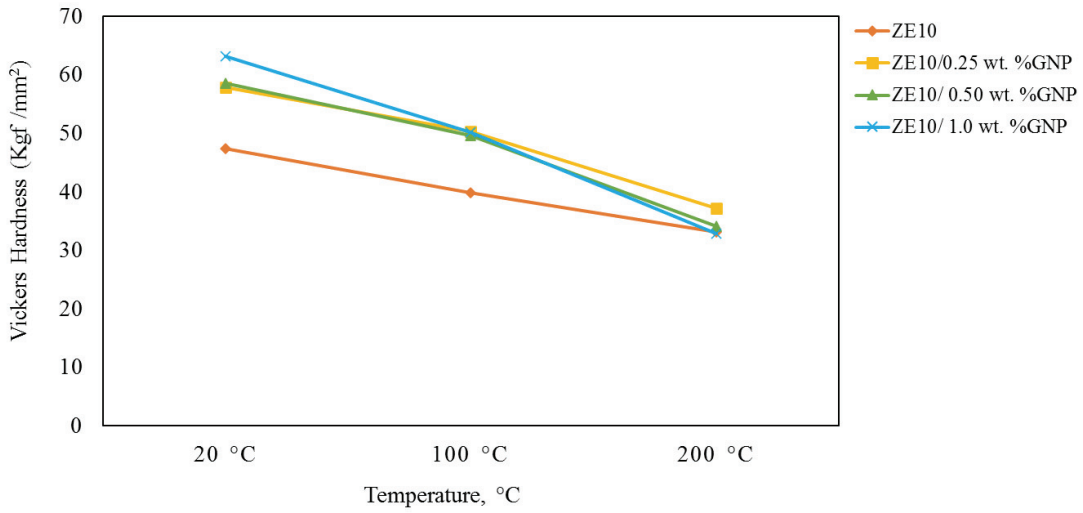

Figure 4.10. Average Vickers hardness values of ZE10 alloy and its composites at RT, 100 °C and 200 °C.

4.2.2. Tensile Test Results

The tensile properties including the average values of 0.2% proof stress (PS), ultimate tensile strength (UTS), and elongation to fracture for the reference alloy and its composites at RT are listed in Table 4.1. In addition to the average test results, the representative tensile stress-strain curves of samples are given in Figure 4.11. The average tensile test result of the ZE10/0.25wt.%GNP composite shows that the 0.2% PS increased by %3 which is not remarkable compared to that of ZE10 reference alloy. However, the PS decreased by 6% and 3% for the ZE10/0.50wt.%GNP and ZE10/1.0wt.%GNP composites, respectively. In addition, the UTS values of composites reinforced with 0.25, 0.5 and 1.0% GNP contents decreased by 15%, 22%, and 24% respectively. It can be suggested that the general trend in diminishing strength with the GNP addition is likely to be due to the grain coarsening. It can be argued that the mechanical properties of composites may be enhanced due to operative Orowan strengthening (addition of nanosized reinforcement) [79]. However, the observed agglomeration sites and porosity may have compensated the strengthening along with the grain coarsening. It is evident that ductility was significantly reduced by the GNP addition. This can be attributed to the clusters of relatively brittle GNP reinforcement and increased porosity (Figure 4.4. b-d).

Table 4.1. Average tensile properties of the ZE10 alloy and its composites at RT.

	0.2%PS (MPa)	UTS (MPa)	Elongation to fracture (%)
ZE10	65±11.08	176±11.06	7.93± 1.88
ZE10/0.25wt.%GNP	67±9.88	148±3.38	4.52±0.61
ZE10/0.5wt.%GNP	61±10	136±9.47	3.93±0.45
ZE10/1.0wt.%GNP	63±7.93	133±3.95	3.51±0.30

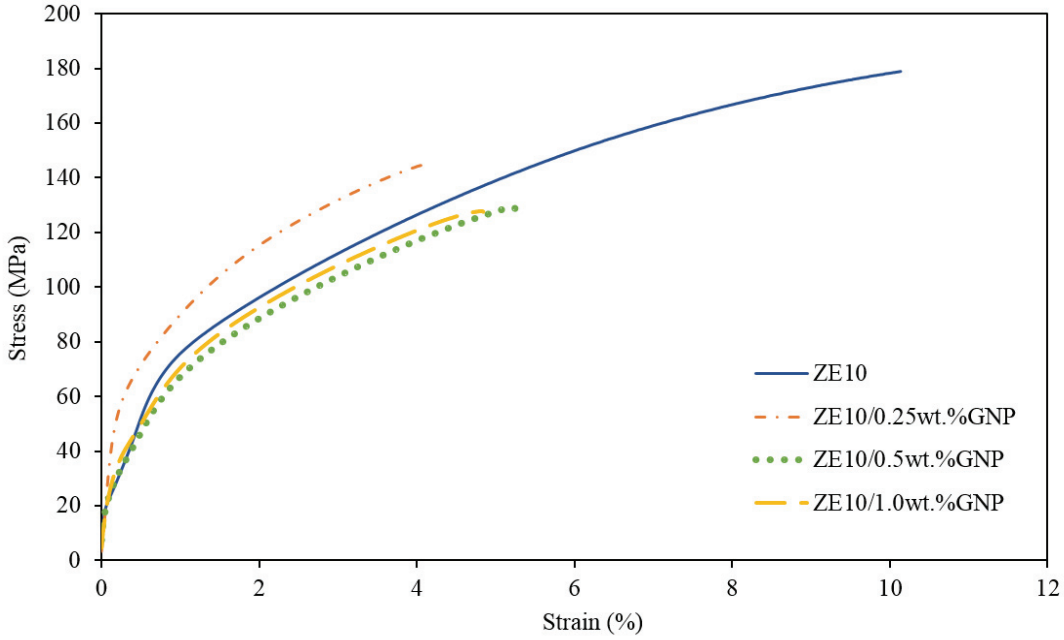

Figure 4.11. Representative stress-strain curves of ZE10 alloy and its composites at RT.

4.2.3. Wear Test

The average COF obtained from the wear tests at various temperatures are seen in Figure 4.12. When the graph of average value COF is examined, the ZE10 alloy and ZE10/1.0wt.%GNP composite have nearly the same COF value at RT. This may suggest that the addition of the GNP content after 0.5wt.% can have no effective influence on the COF value at RT. At 100 °C, in the average of COF values for all samples is increased.

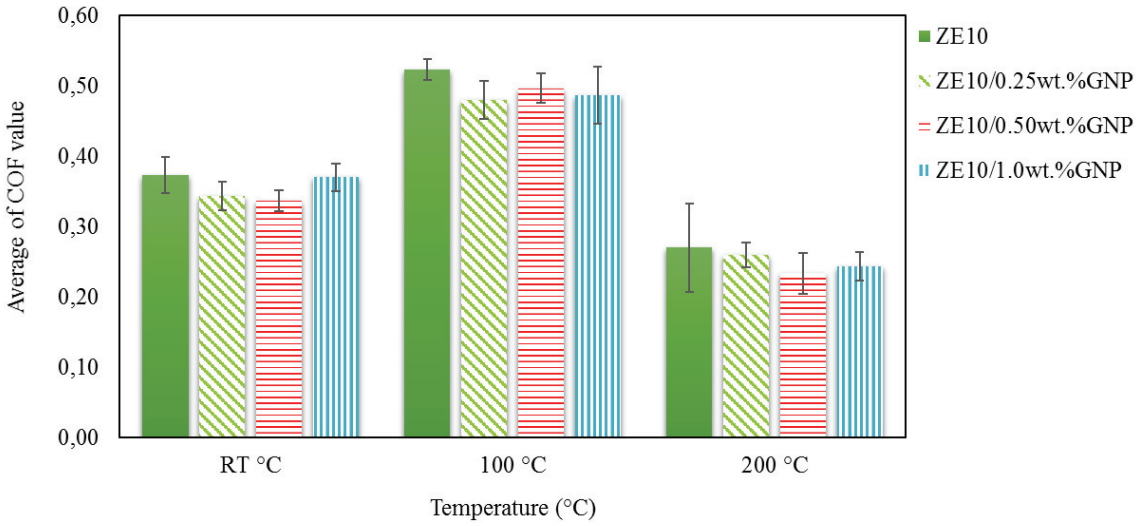

Figure 4.12. Average COF value of ZE10 alloy and its composites at various wear test temperatures.

Figures 4.13, 4.14, and 4.15 show the final COF values of the ZE10 alloy and its composites at RT, 100, and 200 °C. When the ZE10 alloy and composites are compared, the addition of 0.25, 0.5, and 1.0 GNP slightly reduced the COF values by 17%, 15%, and 12% at RT respectively. The composites showed a lower COF than the reference alloy at all temperatures. This can be effect of GNP due to the solid lubricant properties.

An increase in the final COF values is observed in samples at 100 °C compared to the samples tested at RT. The ZE10/0.25wt.%GNP composite has the lowest final COF value at 200 °C. The lack of homogeneous distribution in the microstructure and the increasing amount of pores due to the increasing GNP content could be the reason for the reduced effect of GNP for decreasing COF. The discrepancy in the results could be softening of the matrix at elevated temperature and the pores formed during casting.

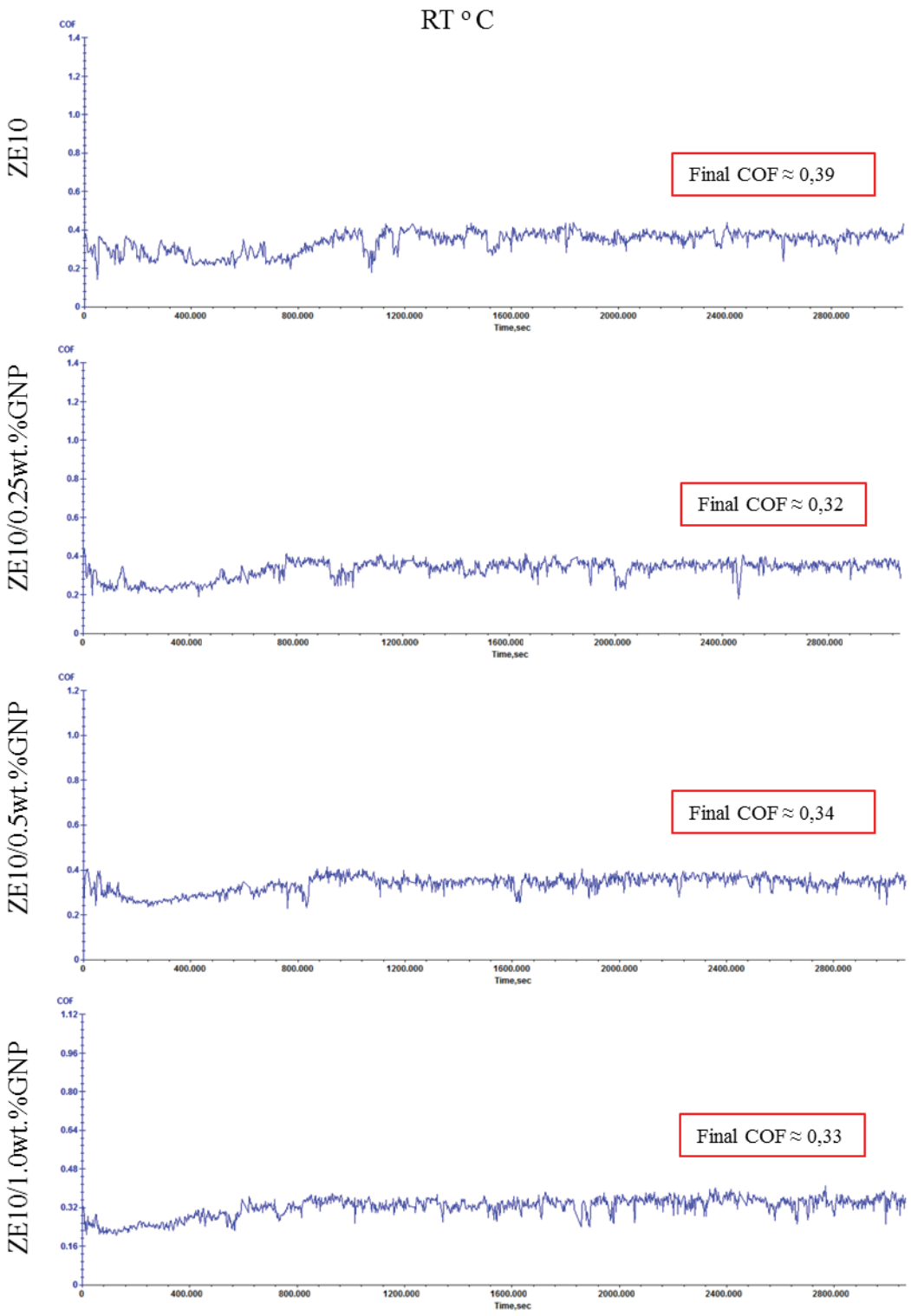

Figure 4.13. Final COF values of ZE10 alloy and its composites at RT.

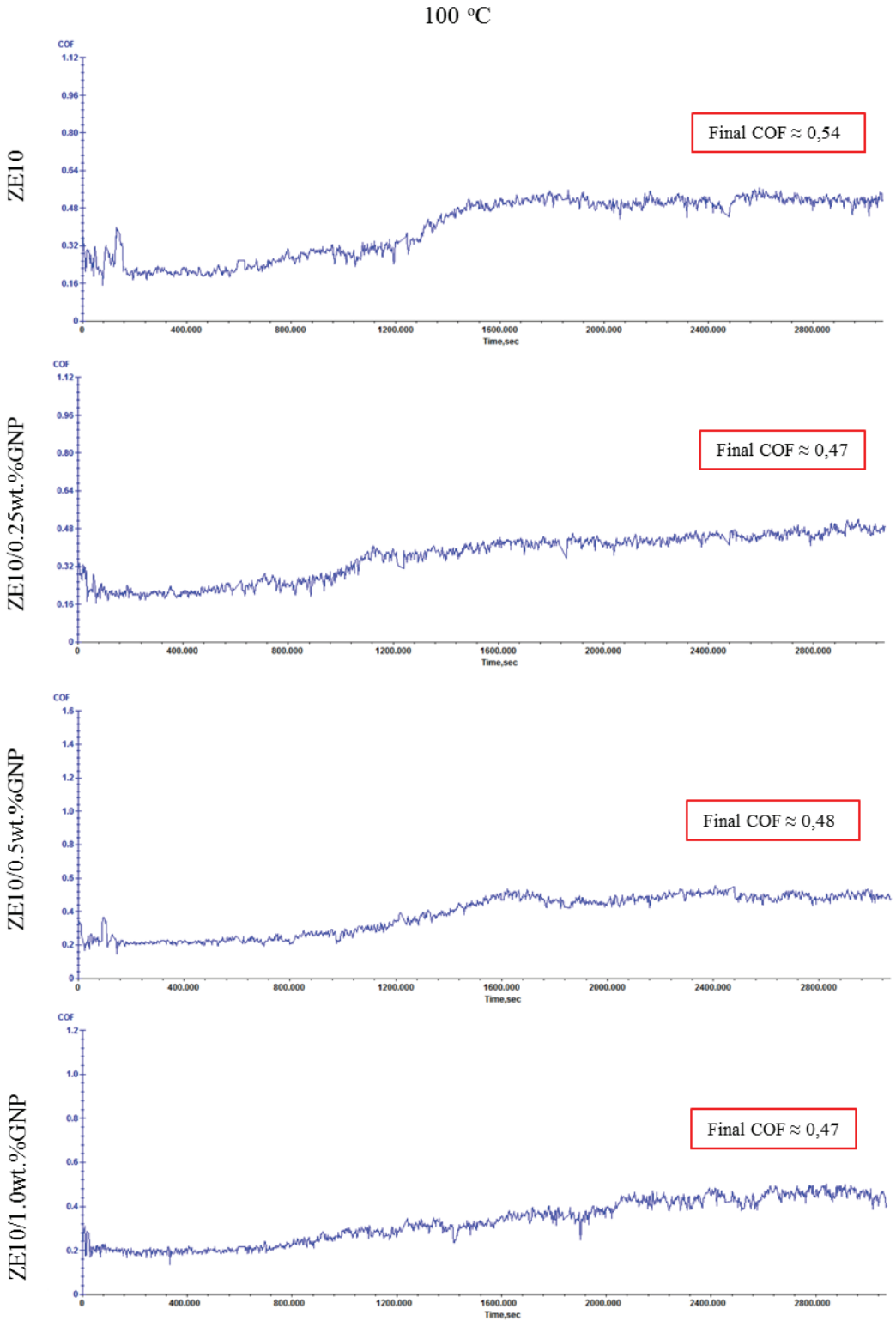

Figure 4.14. Final COF values of ZE10 alloy and its composites at 100 °C.

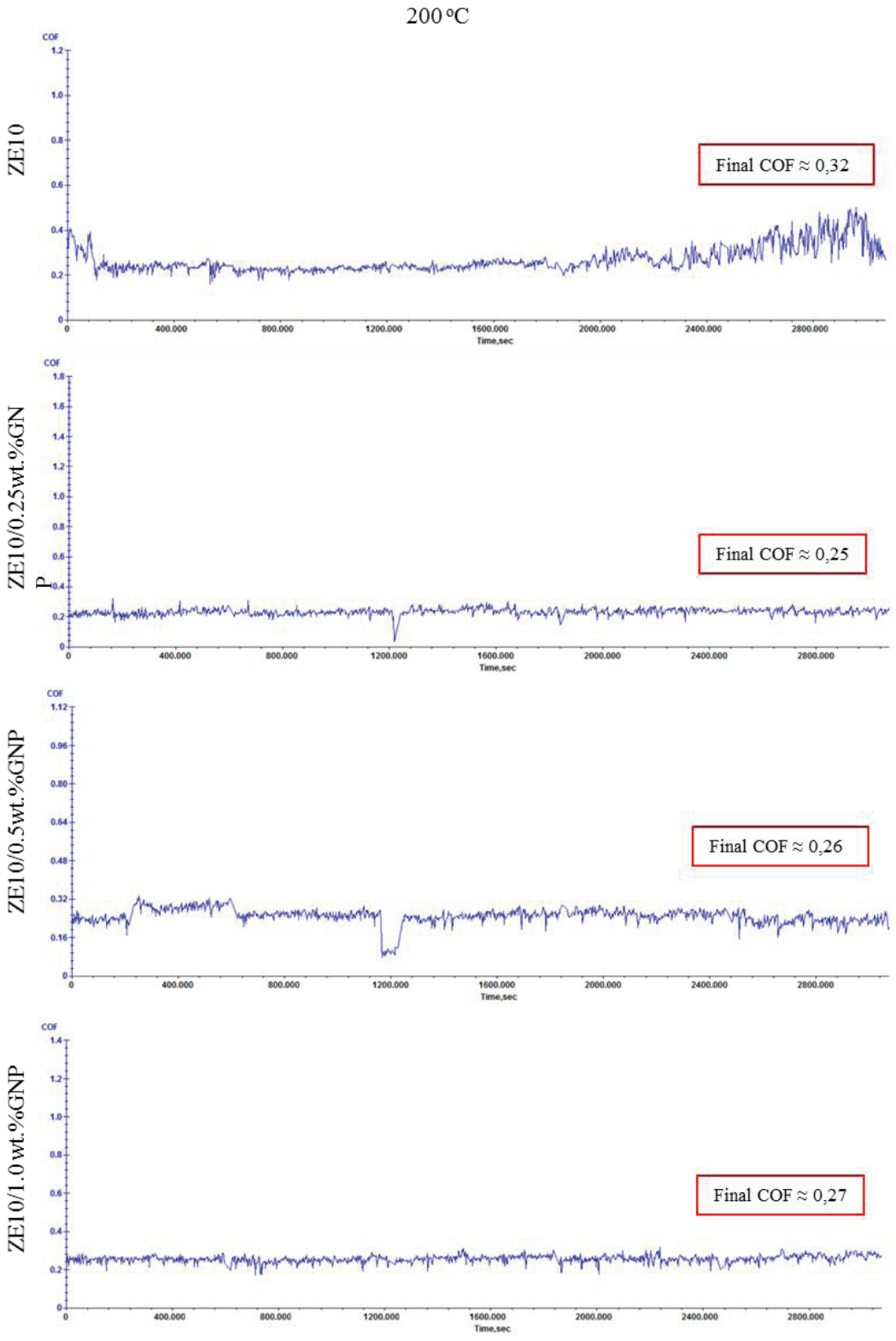

Figure 4.15. Final COF values of ZE10 alloy and its composites at 200 °C.

Figure 4.16 shows average volume losses of ZE10 alloy and its composites at various temperature. ZE10/1.0wt.%GNP has the lowest volume loss at RT, this may be due to the high GNP content. The ZE10/0.25wt.%GNP at 100 °C, and ZE10/0.5wt.%GNP at 200 °C give the lowest volume loss. Volume losses of all samples are reducing with the increasing temperature. The reducing volume losses may be due to the occurrence of plastic deformation by the softening of the matrix.

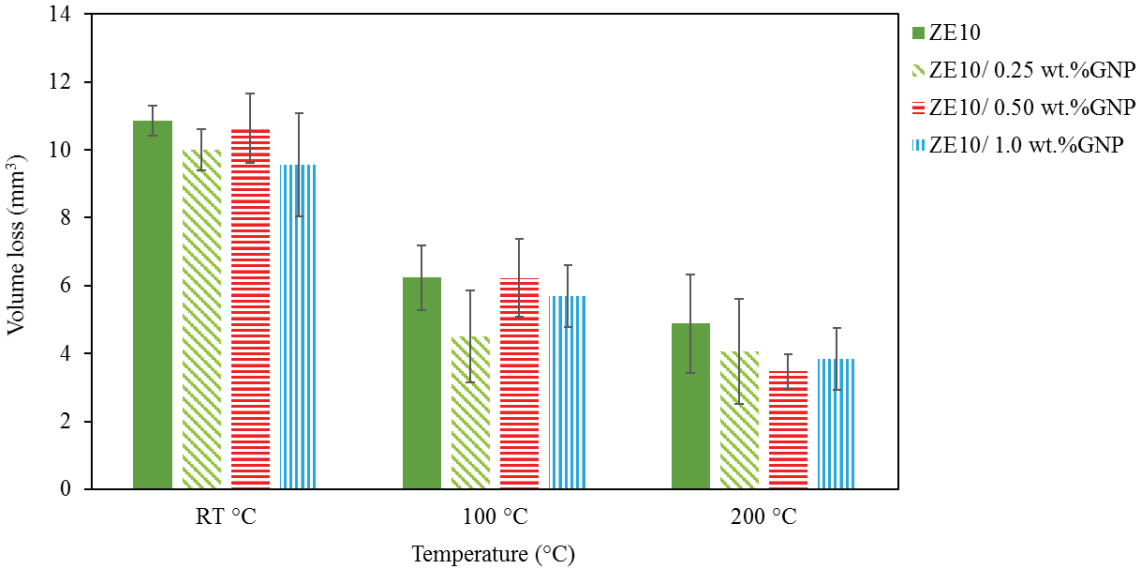

Figure 4.16. Average volume losses of ZE10 alloy and its composites at RT, 100 and 200 °C

4.2.3.1. Analysis of wear scars with SEM

The samples surfaces were analyzed by SEM to determine the wear modes. When the wear surfaces of all samples were investigated at RT, it was revealed that all scratch marks were found to be parallel to the sliding direction.

When examining the samples at RT, wear scar and coated debris to the surface parts of the ZE10 alloy and ZE10/1.0wt.%GNP composite are visible in Figure 4.17. In addition, there are cracks on the surface of the coated debris. While a small amount of coated debris is observed on the wear surface of ZE10/0.25wt.%GNP composite.

In the ZE10/0.25wt.%GNP and ZE10/0.50wt.%GNP composites, there are plowing and wear scars at 100 °C in Figure 4.18. There had increased coated debris in the ZE10/1.0wt.%GNP composite, when the composites at 100 °C temperature were examined. Accumulation and cracking are observed in the surface of coated debris. Wear direction and scars are also more apparent in the ZE10/0.25wt.%GNP and ZE10/0.50wt.%GNP composites at 100 °C.

Coated debris was observed in all samples surface in the wear tests performed at 200 °C (Figure 4.19). However, Coated debris is observed less on the surface of ZE10/0.25wt.%GNP and ZE10/0.50wt.%GNP composites. When the composites were analyzed, it was realized that there are more worn parts adhesion to the surface of the ZE10/1.0wt.%GNP composite. The amount of accumulation on the surface had increased at 200 °C.

The plowing marks, stacking due to the adhesion, and the occurrence of delamination marks on the worn surfaces indicate that the initial mechanism of wear is adhesive wear during the wear test. Additionally, fine furrows and plowing marks on the worn surfaces imply that the other wear mechanism could be the abrasive wear mechanism. Moreover, due to the solid lubricant effect of the GNPs, the surface of ZE10/0.25wt.%GNP nanocomposite have smoother wear scars surface compared to the others. As stated previously, the ZE10/0.25wt.%GNP composite has a more homogeneous GNP distribution.

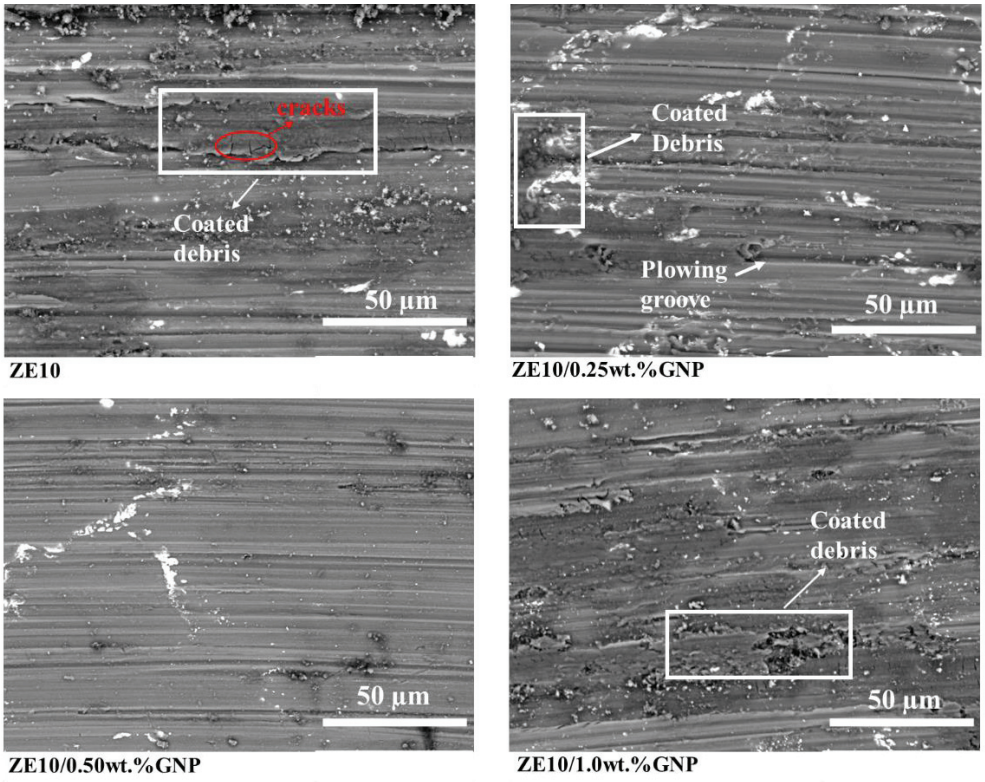

Figure 4.17. SEM micrographs of worn surfaces of ZE10 alloy and its composites at RT.

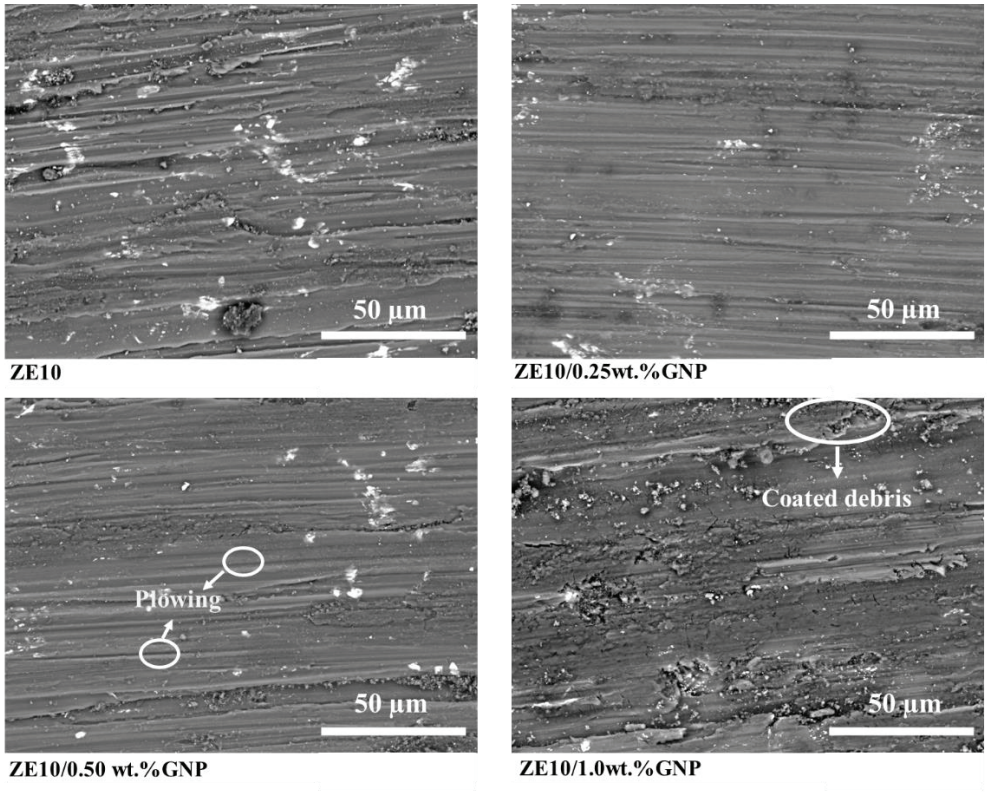

Figure 4.18. SEM micrographs of ZE10 alloy and its composites at 100 °C.

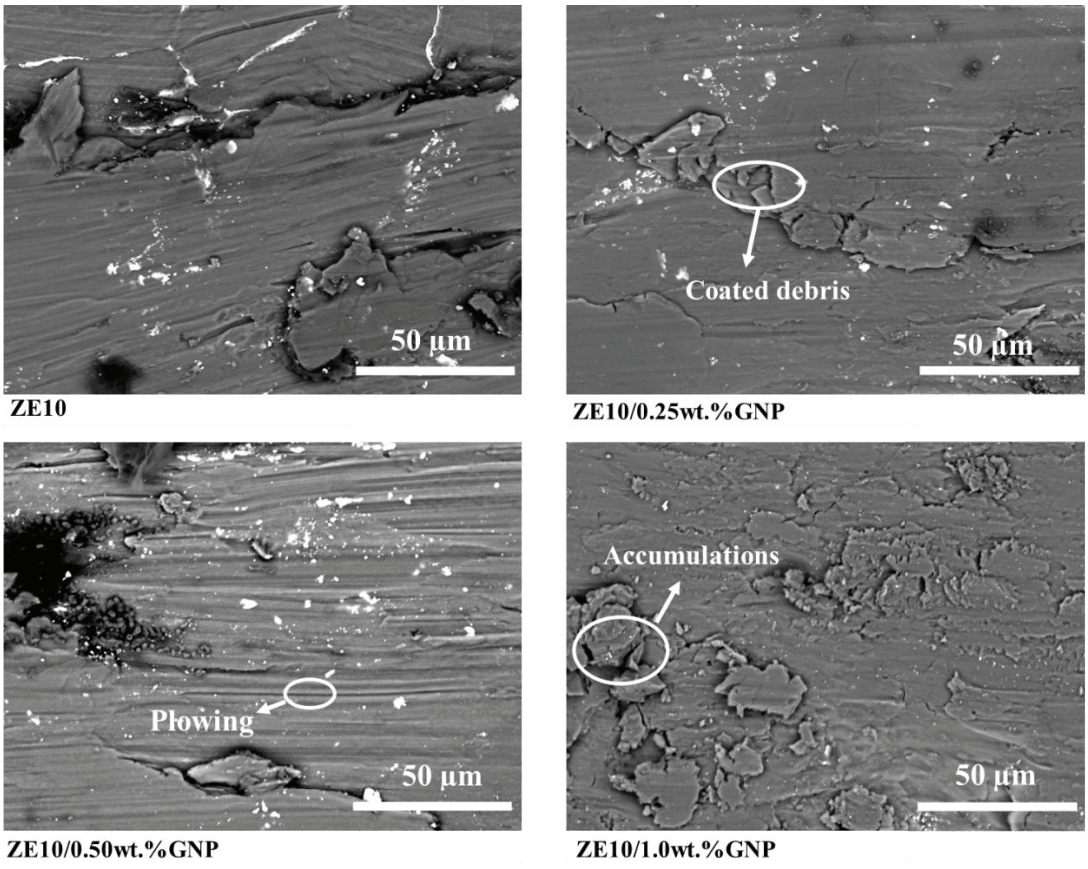

Figure 4.19. SEM micrographs of ZE10 alloy and its composites at 200 °C.

CHAPTER 5

CONCLUSIONS

The mechanical mixing and ultrasonic process applied in the composite fabrication seem to play an effective role in the distribution of GNP in the matrix. The ideal distribution and dispersion of reinforcement into the matrix were obtained in the ZE10/0.25wt.%GNP composite in comparison with the other composites.

The average grain size rose with GNP addition. The grain coarsening was attributed to the inactivation of Zr grain refining effect and the problems associated with homogeneous reinforcement distribution throughout the matrix.

It was observed from the SEM images that the agglomerations and voids tend to increase with increasing GNP content. In the XRD results, the constituents (matrix and GNPs) of the composite did not appear to chemically interact each other. The results of the hardness test suggest that all nanocomposites exhibited better hardness performance than the ZE10 alloy and the ideal GNP content was to be 0.25wt.% in terms of high-temperature hardness properties. The improvement in hardness can be ascribed to the reasonable dispersion of the GNPs into the matrix. The composites have lower UTS values than the unreinforced alloy. It was clear from the average tensile test results that the mechanical properties of composites were not found to be promising due to the presence of GNP clusters and porosity.

Despite the divergent results of average COF value, the composites have lower COF values compared to the ZE10 reference alloy at all temperatures. The lower COF values of composites are likely to be related to the solid lubricant property of GNP. It was observed that all samples have reduced volume losses with increasing temperature. The reducing volume losses may be due to enhanced plastic deformation by softening the matrix at elevated temperatures.

Adhesive and abrasive mechanisms were proposed to be the major wear mechanisms, in consequence of the existence of delicate furrows, coated debris, and plowing marks based on the investigation of the worn surfaces. The worn surface of ZE10/0.25wt.%GNP nanocomposite was found to be smoother than those of other composites which may suggest that it is finer wear performance.

REFERENCES

1. Singh, J., A Review of Major Challenges in the Field of Bagasse Cogeneration in Sugar Mills of India. *Journal: Handbook of Environmental Materials Management* **2019**, 1-32.

2. Tsujimoto, A.; Barkmeier, W. W.; Fischer, N. G.; Nojiri, K.; Nagura, Y.; Takamizawa, T.; Latta, M. A.; Miazaki, M., Wear of resin composites: Current insights into underlying mechanisms, evaluation methods and influential factors. *Japanese Dental Science Review* **2018,** *54* (2), 76-87.

3. Kulekci, M. K., Magnesium and its alloys applications in automotive industry. *The International Journal of Advanced Manufacturing Technology* **2008,** *39* (9-10), 851-865.

4.Faruk, O.; Tjong, J.; Sain, M., *Lightweight and sustainable materials for automotive applications*. CRC Press Boca Raton: 2017.

5. Cole, G.; Sherman, A., Lightweight Materials for Automotive Applications, 1995. Elsevier.

6. Chawla, N.; Shen, Y.-L., Mechanical Behavior of Particle Reinforced Metal Matrix Composites. *Advanced Engineering Materials* **2001,** *3* (6), 357-370.

7. Selvam, J. D.; Dinaharan, I.; Rai, R. S., Matrix and Reinforcement Materials for Metal Matrix Composites. **2021**.

8. Gupta, M.; Wong, W., Magnesium-based nanocomposites: Lightweight materials of the future. *Materials Characterization* **2015,** *105*, 30-46.

9. Güler, Ö.; Bağcı, N., A short review on mechanical properties of graphene reinforced metal matrix composites. *Journal of Materials Research and Technology* **2020,** *9* (3), 6808-6833.

10. Berman, D.; Erdemir, A.; Sumant, A. V., Graphene: a new emerging lubricant. *Materials Today* **2014,** *17* (1), 31-42.

11. Malaki, M.; Fadaei Tehrani, A.; Niroumand, B.; Gupta, M., Wettability in Metal Matrix Composites. *Metals* **2021,** *11* (7), 1034.

12. Ceschini, L.; Dahle, A.; Gupta, M.; Jarfors, A. E. W.; Jayalakshmi, S.; Morri, A.; Rotundo, F.; Toschi, S.; Singh, R. A., *Aluminum and magnesium metal matrix nanocomposites*. Springer: 2017.

13. Chawla, K. K., Metal matrix composites. In *Composite materials*, Springer: 2012; pp 197-248.

14. Gavalda Diaz, O.; Garcia Luna, G.; Liao, Z.; Axinte, D., The new challenges of machining Ceramic Matrix Composites (CMCs): Review of surface integrity. *International Journal of Machine Tools and Manufacture* **2019,** *139*, 24-36.

15. Mistry, J. M.; Gohil, P. P., Research review of diversified reinforcement on aluminum metal matrix composites: fabrication processes and mechanical characterization. *Science and Engineering of Composite Materials* **2018,** *25* (4), 633-647.

16. Tjong, S.; Ma, Z., Microstructural and mechanical characteristics of in situ metal matrix composites. *Materials Science and Engineering: R: Reports* **2000,** *29* (3-4), 49-113.

17. Aylor, D. M.; Moran, P. J., Effect of reinforcement on the pitting behavior of aluminum-base metal matrix composites. *Journal of the Electrochemical Society* **1985,** *132* (6), 1277.

18. Şenel, M. C.; Gürbüz, M.; Erdem, K., Grafen takviyeli alüminyum matrisli yeni nesil kompozitler. *Mühendis ve Makina* **2015,** *56* (669), 36-47.

19. Rashad, M.; Pan, F.; Tang, A.; Lu, Y.; Asif, M.; Hussain, S.; She, J.; Gou, J.; Mao, J., Effect of graphene nanoplatelets (GNPs) addition on strength and ductility of magnesium-titanium alloys. *Journal of Magnesium and Alloys* **2013,** *1* (3), 242-248.

20. Ahmad, S. I.; Hamoudi, H.; Abdala, A.; Ghouri, Z. K.; Youssef, K. M., Graphene-reinforced bulk metal matrix composites: synthesis, microstructure, and properties. *Reviews on Advanced Materials Science* **2020,** *59* (1), 67-114.

21. Alipour, M.; Eslami-Farsani, R., Synthesis and characterization of graphene nanoplatelets reinforced AA7068 matrix nanocomposites produced by liquid metallurgy route. *Materials Science and Engineering: A* **2017,** *706*, 71-82.

22. Baradeswaran, A.; Elaya Perumal, A., Effect of graphite on tribological and mechanical properties of AA7075 composites. *Tribology Transactions* **2015,** *58* (1), 1-6.

23. Shanmughasundaram, P.; Subramanian, R., Wear behaviour of eutectic Al-Si alloy-graphite composites fabricated by combined modified two-stage stir casting and squeeze casting methods. *Advances in materials science and engineering* **2013,** *2013*.

24. Chen, L.-Y.; Peng, J.-Y.; Xu, J.-Q.; Choi, H.; Li, X.-C., Achieving uniform distribution and dispersion of a high percentage of nanoparticles in metal matrix nanocomposites by solidification processing. *Scripta materialia* **2013,** *69* (8), 634-637.

25. Abbas, A.; Huang, S. J.; Ballokova, B.; Sülleiová, K., Tribological effects of carbon nanotubes on magnesium alloy AZ31 and analyzing aging effects on CNTs/AZ31 composites fabricated by stir casting process. *Tribology International* **2020,** *142*, 105982.

26. Wu, L.; Wu, R.; Hou, L.; Zhang, J.; Zhang, M., Microstructure, mechanical properties and wear performance of AZ31 matrix composites reinforced by graphene nanoplatelets (GNPs). *Journal of Alloys and Compounds* **2018,** *750*, 530-536.

27. Plachá, D.; Jampilek, J., Graphenic Materials for Biomedical Applications. *Nanomaterials* **2019,** *9* (12), 1758.

28. Chiou, Y.-C.; Chou, H.-Y.; Shen, M.-Y., Effects of adding graphene nanoplatelets and nanocarbon aerogels to epoxy resins and their carbon fiber composites. *Materials & Design* **2019,** *178*, 107869.

29. Yu, W.; Sisi, L.; Haiyan, Y.; Jie, L., Progress in the functional modification of graphene/graphene oxide: A review. *RSC Advances* **2020,** *10* (26), 15328-15345.

30. Rashad, M.; Pan, F. S.; Asif, M.; Ullah, A., Improved mechanical properties of magnesium–graphene composites with copper–graphene hybrids. *Materials Science and Technology* **2015,** *31* (12), 1452-1461.

31. Arab, M.; Marashi, S., Effect of graphene nanoplatelets (GNPs) content on improvement of mechanical and tribological properties of AZ31 Mg matrix nanocomposite. *Tribology International* **2019,** *132*, 1-10.

32. Chen, L.-Y.; Konishi, H.; Fehrenbacher, A.; Ma, C.; Xu, J.-Q.; Choi, H.; Xu, H.-F.; Pfefferkorn, F. E.; Li, X.-C., Novel nanoprocessing route for bulk graphene nanoplatelets reinforced metal matrix nanocomposites. *Scripta Materialia* **2012,** *67* (1), 29-32.

33. Das, A.; Harimkar, S. P., Effect of graphene nanoplate and silicon carbide nanoparticle reinforcement on mechanical and tribological properties of spark plasma sintered magnesium matrix composites. *Journal of Materials Science & Technology* **2014,** *30* (11), 1059-1070.

34. Casati, R., *Aluminum matrix composites reinforced with alumina nanoparticles*. Springer: 2016.

35. Polat, S. Alümnyum matrisli grafen ve seramik takviyeli kompozitlerin mekanik ve termal özelliklerinin incelenmesi. 2020.

36. Anish, R.; Singh, G. R.; Sivapragash, M., Techniques for processing metal matrix composite; A survey. *Procedia engineering* **2012,** *38*, 3846-3854.

37. GG, S.; S Balasivanandha, P.; VSK, V., Effect of processing paramters on metal matrix composites: stir casting process. *Journal of Surface Engineered Materials and advanced technology* **2012,** *2012*.

38. Nishida, Y., *Introduction to metal matrix composites: fabrication and recycling*. Springer Science & Business Media: 2013.

39. Cooke, K. O., A study of the effect of nanosized particles on transient liquid phase diffusion bonding Al6061 metal–matrix composite (MMC) using Ni/Al 2 O 3 nanocomposite interlayer. *Metallurgical and Materials Transactions B* **2012,** *43* (3), 627-634.

40. Shah, D. M.; Anton, D. L., In-Situ Synthesis of Intermetallic Matrix Composites. *MRS Online Proceedings Library (OPL)* **1992,** *273*.

41. Singla, M.; Dwivedi, D. D.; Singh, L.; Chawla, V., Development of aluminium based silicon carbide particulate metal matrix composite. *Journal of Minerals and Materials Characterization and Engineering* **2009,** *8* (06), 455.

42. Anthymidis, K.; David, K.; Agrianidis, P.; Trakali, A. In *Production of Al metal matrix composites by the stir-casting method*, Key engineering materials, Trans Tech Publ: 2014; pp 614-617.

43. Matin, A.; Saniee, F. F.; Abedi, H. R., Microstructure and mechanical properties of Mg/SiC and AZ80/SiC nano-composites fabricated through stir casting method. *Materials Science and Engineering: A* **2015,** *625*, 81-88.

44. Ghauri, K. M.; Ali, L.; Ahmad, A.; Ahmad, R.; Din, K. M.; Chaudhary, I. A.; Karim, R. A., Synthesis and characterization of Al/SiC composite made by stir casting method. *Pakistan Journal of Engineering and Applied Sciences* **2013**.

45. Poddar, P.; Srivastava, V. C.; De, P. K.; Sahoo, K. L., Processing and mechanical properties of SiC reinforced cast magnesium matrix composites by stir casting process. *Materials Science and Engineering: A* **2007,** *460-461*, 357-364.

46. Hashim, J.; Looney, L.; Hashmi, M. S. J., Metal matrix composites: production by the stir casting method. *Journal of Materials Processing Technology* **1999,** *92-93*, 1-7.

47. Nie, K.; Wang, X.; Wu, K.; Xu, L.; Zheng, M.; Hu, X., Processing, microstructure and mechanical properties of magnesium matrix nanocomposites fabricated by semisolid stirring assisted ultrasonic vibration. *Journal of alloys and compounds* **2011,** *509* (35), 8664-8669.

48. Prasad, S. V. S.; Prasad, S. B.; Verma, K.; Mishra, R. K.; Kumar, V.; Singh, S., The role and significance of Magnesium in modern day research-A review. *Journal of Magnesium and Alloys* **2022,** *10* (1), 1-61.

49. Seetharam, R.; Madhukar, P.; Yoganjaneyulu, G.; Subbu, S. K.; Davidson, M. J., Mathematical Models to Predict Flow Stress and Dynamically Recrystallized Grain Size of Deformed AA7150-5 wt% B4C Composite Fabricated Using Ultrasonic-Probe Assisted Stir Casting Process. *Metals and Materials International* **2021**.

50. Idrisi, A. H.; Mourad, A.-H. I., Conventional stir casting versus ultrasonic assisted stir casting process: Mechanical and physical characteristics of AMCs. *Journal of Alloys and Compounds* **2019,** *805*, 502-508.

51. Khandelwal, A.; Mani, K.; Srivastava, N.; Gupta, R.; Chaudhari, G. P., Mechanical behavior of AZ31/Al2O3 magnesium alloy nanocomposites prepared using ultrasound assisted stir casting. *Composites Part B: Engineering* **2017,** *123*, 64-73.

52. Nie, K.; Wang, X.; Wu, K.; Hu, X.; Zheng, M., Development of SiCp/AZ91 magnesium matrix nanocomposites using ultrasonic vibration. *Materials Science and Engineering: A* **2012,** *540*, 123-129.

53. Hashim, J.; Looney, L.; Hashmi, M. S. J., The wettability of SiC particles by molten aluminium alloy. *Journal of Materials Processing Technology* **2001,** *119* (1), 324-328.

54. Abdulla, F. A.; Moustafa, N. M.; Al-Ameen, E. S., Calculation of Wear Rate by Weight and Volume for Aluminum Samples. *Journal of University of Babylon for Engineering Sciences* **2018,** *26* (7), 331-339.

55. Meng, H.; Ludema, K., Wear models and predictive equations: their form and content. *Wear* **1995,** *181*, 443-457.

56. Khedkar, J.; Negulescu, I.; Meletis, E. I., Sliding wear behavior of PTFE composites. *Wear* **2002,** *252* (5-6), 361-369.

57. Shanmughasundaram, P.; Subramanian, R., Wear Behaviour of Eutectic Al-Si Alloy-Graphite Composites Fabricated by Combined Modified Two-Stage Stir Casting and Squeeze Casting Methods. *Advances in Materials Science and Engineering* **2013,** *2013*, 216536.

58. Suh, N. P., The delamination theory of wear. *Wear* **1973,** *25* (1), 111-124.

59. Morshed, A.; Wu, H.; Jiang, Z., A Comprehensive Review of Water-Based Nanolubricants. *Lubricants* **2021,** *9* (9), 89.

60. Radhika, N.; Raghu, R.; Vidyapeetham, A., Synthesis of functionally graded aluminium composite and investigation on its abrasion wear behaviour. *Journal of Engineering Science and Technology* **2017,** *12* (5), 1386-1398.

61. Ashrafizadeh, H.; McDonald, A.; Mertiny, P., Erosive and abrasive wear resistance of polyurethane liners. *Aspects of polyurethanes* **2017,** *6*, 131.

62. Kavimani, V.; Prakash, K. S.; Thankachan, T., Surface characterization and specific wear rate prediction of r-GO/AZ31 composite under dry sliding wear condition. *Surfaces and Interfaces* **2017,** *6*, 143-153.

63. Zhu, J.; Qi, J.; Guan, D.; Ma, L.; Dwyer-Joyce, R., Tribological behaviour of self-lubricating Mg matrix composites reinforced with silicon carbide and tungsten disulfide. *Tribology International* **2020,** *146*, 106253.

64. Zhao, Z.; Bai, P.; Du, W.; Liu, B.; Pan, D.; Das, R.; Liu, C.; Guo, Z., An overview of graphene and its derivatives reinforced metal matrix composites: preparation, properties and applications. *Carbon* **2020**.

65. Jeon, C.-H.; Jeong, Y.-H.; Seo, J.-J.; Tien, H. N.; Hong, S.-T.; Yum, Y.-J.; Hur, S.-H.; Lee, K.-J., Material properties of graphene/aluminum metal matrix composites fabricated by friction stir processing. *International journal of precision engineering and manufacturing* **2014,** *15* (6), 1235-1239.

66. Ramesh, S.; Govindaraju, N.; Suryanarayan, C. In *Investigation on mechanical and fatigue behaviour of aluminium based SiC/ZrO2 particle reinforced MMC*, IOP conference series: materials science and engineering, IOP Publishing: 2018; p 012030.

67. Arab, M.; Marashi, S., Graphene nanoplatelet (GNP)-incorporated AZ31 magnesium nanocomposite: microstructural, mechanical and tribological properties. *Tribology Letters* **2018,** *66* (4), 1-11.

68. Du, X.; Du, W.; Wang, Z.; Liu, K.; Li, S., Ultra-high strengthening efficiency of graphene nanoplatelets reinforced magnesium matrix composites. *Materials Science and Engineering: A* **2018,** *711*, 633-642.

69. Kandemir, S., Development of graphene nanoplatelet-reinforced AZ91 magnesium alloy by solidification processing. *Journal of Materials Engineering and Performance* **2018,** *27* (6), 3014-3023.

70. Rashad, M.; Pan, F.; Hu, H.; Asif, M.; Hussain, S.; She, J., Enhanced tensile properties of magnesium composites reinforced with graphene nanoplatelets. *Materials Science and Engineering: A* **2015,** *630*, 36-44.

71. Song, J. F.; Dieringa, H.; Huang, Y. D.; Gan, W. M.; Kainer, K. U.; Hort, N. In *Mechanical properties and microstructures of nano SiC reinforced ZE10 composites prepared with ultrasonic vibration*, Advanced Materials Research, Trans Tech Publ: 2014; pp 169-176.

72. Haghshenas, M.; Gupta, M., Magnesium nanocomposites: An overview on time-dependent plastic (creep) deformation. *Defence Technology* **2019,** *15* (2), 123-131.

73. Dieringa, H.; Hort, N.; Kainer, K. In *Ultrasonic stirring as a production process for nanoparticle reinforced magnesium alloys and the compression creep response of ZE10 reinforced with ceria nanoparticles*, 15th European Conference on Composite Materials, Venice, Italy, 2012.

74. Ramezani, M.; Neitzert, T.; Pasang, T.; Sellès, M., Characterization of friction behaviour of AZ80 and ZE10 magnesium alloys under lubricated contact condition by strip draw and bend test. *International Journal of Machine Tools and Manufacture* **2014,** *85*, 70-78.

75. Liu, Y.; Li, W.; Li, Y.-y., Microstructure and mechanical properties of ZE10 magnesium alloy prepared by equal channel angular pressing. *International Journal of Minerals, Metallurgy and Materials* **2009,** *16* (5), 559-563.

76. Podymova, N. B.; Karabutov, A. A., Combined effects of reinforcement fraction and porosity on ultrasonic velocity in SiC particulate aluminum alloy matrix composites. *Composites Part B: Engineering* **2017,** *113*, 138-143.

77. Callister Jr, W. D.; Rethwisch, D. G., *Fundamentals of materials science and engineering: an integrated approach*. John Wiley & Sons: 2020.

78. Lim, H.; Hoag, S. W., Plasticizer effects on physical–mechanical properties of solvent cast Soluplus® films. *Aaps Pharmscitech* **2013,** *14* (3), 903-910.

79. Zhang, Z.; Chen, D., Consideration of Orowan strengthening effect in particulate-reinforced metal matrix nanocomposites: A model for predicting their yield strength. *Scripta materialia* **2006,** *54* (7), 1321-1326.